Hierarchization of polyion complex vesicle for mimicry of cellular organelles

Maruyama, Tomoki
Katayama lab, Graduate School of Systems Life Sciences, Kyushu University

DISSERTATION

for Master's Degree

Hierarchization of polyion complex vesicle for mimicry of cellular organelles

細胞内オルガネラの構造を模倣した

ポリイオンコンプレックスベシクルの階層化

Katayama lab

Graduate School of Systems Life Sciences

Kyushu University

Tomoki Maruyama

Supervisor

Assoc. Prof. Akihiro Kishimura

Acknowledgement

I would first like to thank my supervisor Assoc. Prof. Akihiro Kishimura for his guidance through each stage of the process. I would also like to acknowledge Prof. Yoshiki Katayama and Assoc. Prof. Takeshi Mori for their valuable advice and suggestions.

I would like to express my appreciation to Mr. Yiwei Liu, Ms. Asmariah Ahmad, Mr. Biplab K.C. and Mr. Chan MengJu for their guidance, advice and support. Especially, Mr. Yiwei Liu, Mr. Biplab K.C. and Mr. Chan MengJu taught me a lot of experimental skills and knowledge. Ms. Asmariah Ahmad helped me a lot to improve my English skill and mentally supported me when I faced hard time. Also, Mr. Biplab K.C. led me to the fantastic world of coacervate, which I got very excited about.

I would like to express my sincere gratitude to Prof. (ret.) Atsushi Takahara for their technical support on the sample preparation for cross-sectional TEM, Prof. Masaharu Murata and Asst. Prof. Takahito Kawano for their technical support on FCS measurement, as well as Nanotechnology Platform, Applied Chemistry, Kyushu University for allowing me to conduct TEM observation and NMR measurement.

Finally, I am very thankful to all of my friends and family for supporting me on this journey.

Abstract

Polyion complexes (PICs) are self-assembly formed from oppositely charged polyelectrolytes via electrostatic interaction. PICs are known to form a variety of structures such as micelle, vesicle and coacervate depending on polymer characteristics and/or environmental condition in a facile and controlled manner, which makes them attractive system for developing hierarchical structures. Of such structures, this work is mainly focused on vesicle, also known as PICsome formed by exploiting PEG-based di-block copolymer and coacervate, which is formed through liquid liquid phase separation (LLPS) process. By utilizing PICsome and coacervate as a fundamental structure, two types of hierarchical PIC structures are explored; (i) multilamellar PICsome, in which two or more PICsomes are integrated by tuning environmental condition and (ii) coacervate-in-PICsome, in which PICsome and coacervate are integrated by tuning the polymer characteristics. The formation mechanism and regulation principle of multilamellar PICsome and coacervate-in-PICsome are also investigated for further controllability of the structures as well as the functionalities. The work done in this study will pave the way toward constructing a variety of highly organized PIC structures with excellent functionalities, which can be a novel artificial organelle.

Contents

Chapter 1 Introduction

1-1. Cellular organelles

Cells contain a variety of cellular organelles such as nucleus [1], mitochondria [2], endoplasmic reticulum [3], Golgi apparatus [4] and so on to perform complex biochemical processes in a highly controlled manner by endowing specific roles to each organelle. Some of the cellular organelles have a highly organized structure, which plays an important role to their outstanding functions. For example, mitochondria are composed of two membranes: inner mitochondrial membrane (IMM) and outer mitochondrial membrane (OMM) (Figure 1A), which are structurally and functionally distinct. The IMM is mainly responsible for energy conversion, on the other hand, the OMM is the platform for cell signaling events [2]. Nucleus is also one of the structurally hierarchized cellular organelles. It contains a number of biomolecular condensates, which are physically compartmentalized from cytoplasm by a membrane (Figure 1B) and provides the distinct environment for molecular processing or storage [1].

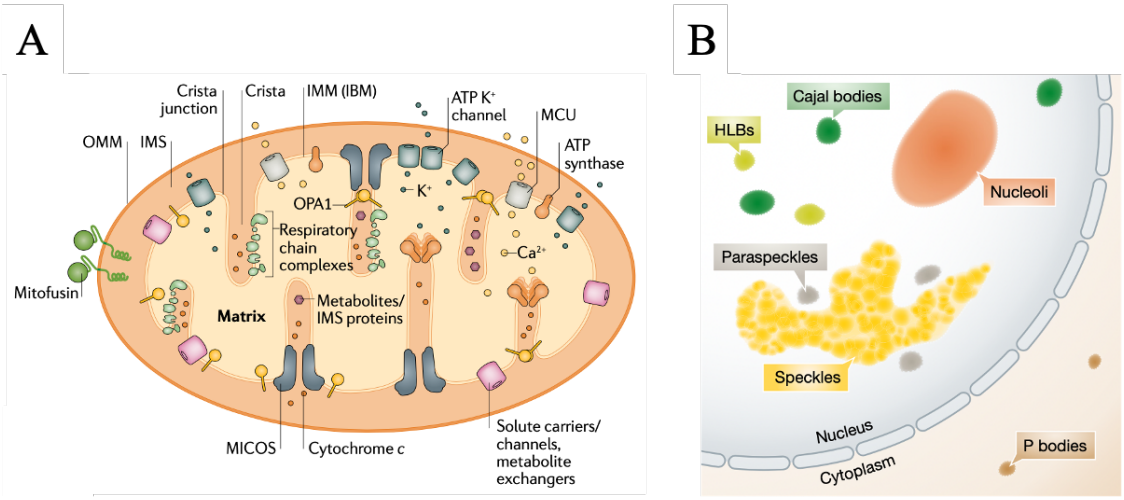

Figure 1. Schematic illustration of (A) mitochondria (Adopted from reference [2]) and (B) nucleus (Adopted from reference [1]).

1-2. Artificial organelles

Reconstruction of artificial organelles by mimicking structures or functions of cellular organelles is one of the most powerful ways not only to understand the biological functions of cellular organelles but also to create a highly functionalized biomaterials for a wide range of applications. In particular, bottom-up approach has gained much attention in the field of synthetic biology since it provides a simplified model to elaborate cells and enables to design the structures or tailer the functions of artificial analogs [5]. Based on bottom-up approach, two types of structures formed via molecular self-assembly process have been extensively studied so far; vesicle and coacervate (Figure 2). Vesicle is a membrane-bound compartment, physically separating its inner space from the outer environment, on the other hand, coacervate is a membraneless liquid droplet formed through liquid liquid phase separation (LLPS) process [6,7]. Both of them have shown their potentials as an artificial organelle, which can demonstrate a range of functionalities [8-16]. However, it is still challenging to create artificial organelles with hierarchical structures similar to the structure of mitochondria or nucleus as mentioned above although it enables to perform more complex and highly regulated functionalities.

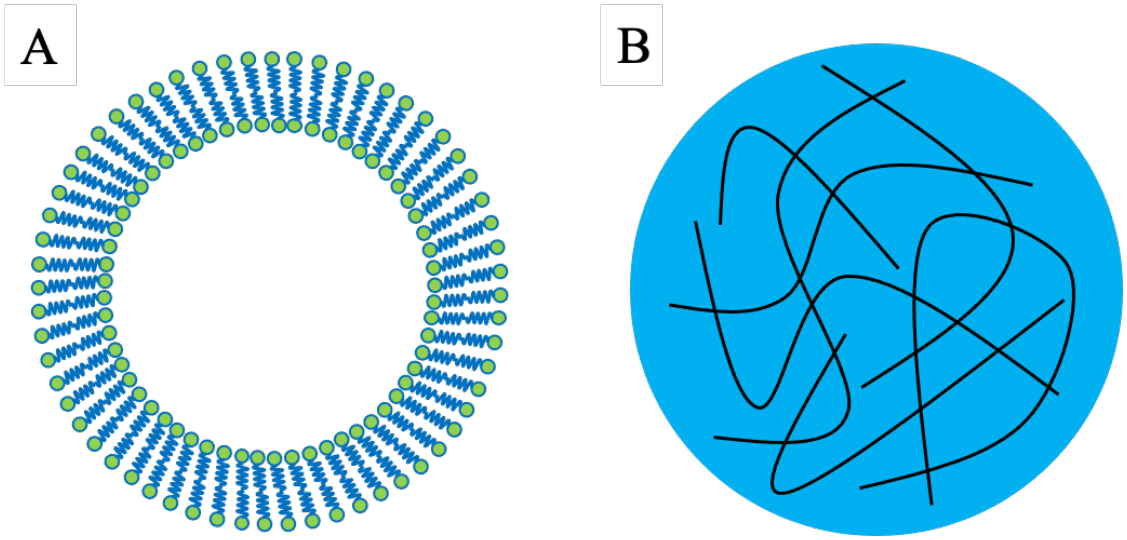

Figure 2. Schematic illustration of the structure of (A) vesicle and (B) coacervate.

1-3. Polyion complexes (PICs)

Polyion complexes (PICs) are self-assembly which is spontaneously formed based on electrostatic interaction between oppositely charged polymers, ranging from natural polymers such as nucleic acids or proteins to synthetic polymers [17-20]. Especially, when it comes to synthetic polymer, which can be advantageous for controlling morphological and material properties of the resultant assembly, a variety of structures including micelle, vesicle and coacervate are known to be formed, for example by utilizing di-block copolymer composed of neutral block and charged block [21] and/or by tuning the environment of the system such as pH [22], ionic strength [23], temperature [24] and so forth (Figure 3). Considering the simplicity of its preparation and the structural controllability, PIC system can be considered promising for constructing the hierarchical structures.

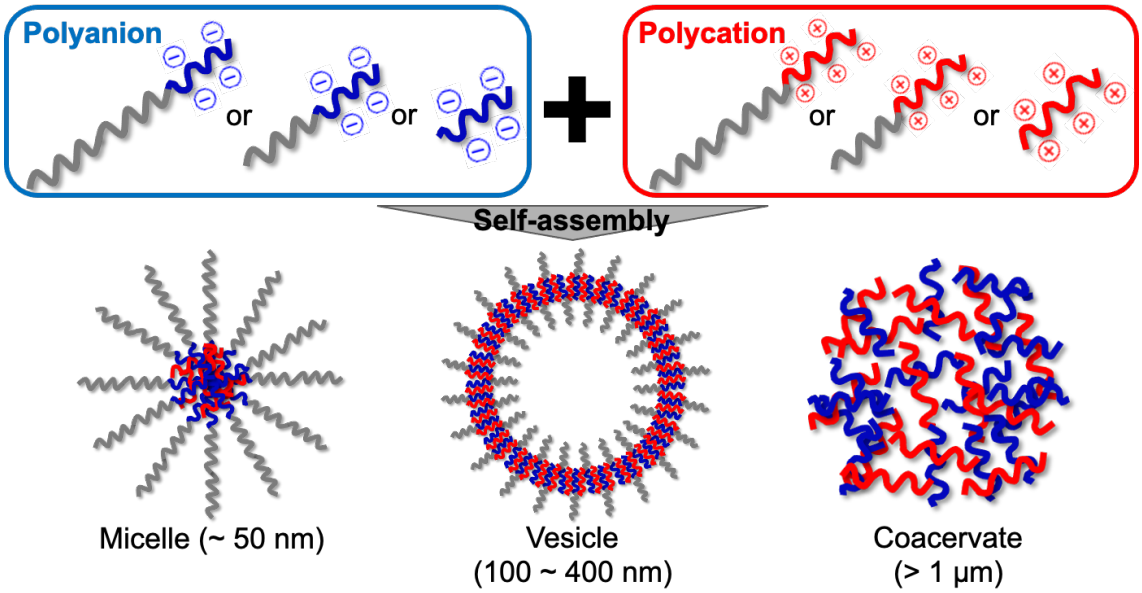

Figure 3. Various structures formed from synthetic polyelectrolytes depending on polymer characteristics and environmental condition.

1-4. Polyion complex vesicle (PICsome)

Among above mentioned PICs, vesicle structure called PICsome has been gaining much attention due to its morphological similarity with cellular organelles, i.e. membrane bound structure in the field of bottom-up synthetic biology. PICsome can be prepared by mixing poly(ethylene glycol) (PEG) based polyanion and homo-polycation, resulting in the unilamellar membrane formation, in which PIC layer is sandwiched by PEG layers (Figure 4). Previous studies showed that PICsome has unique properties such as controllable size, hydrophilic and semi-permeable membrane, etc. and these properties can be fine-tuned [25-33]. In addition, it has been demonstrated that enzymatic reaction can take place inside PICsome, where substrates penetrate the membrane and react with enzymes encapsulated into the hollow space [34-36]. Given these identical characteristics of PICsome mentioned above, utilization of PICsome as a platform for hierarchizing PIC structure is a promising way for creating functional artificial organelles.

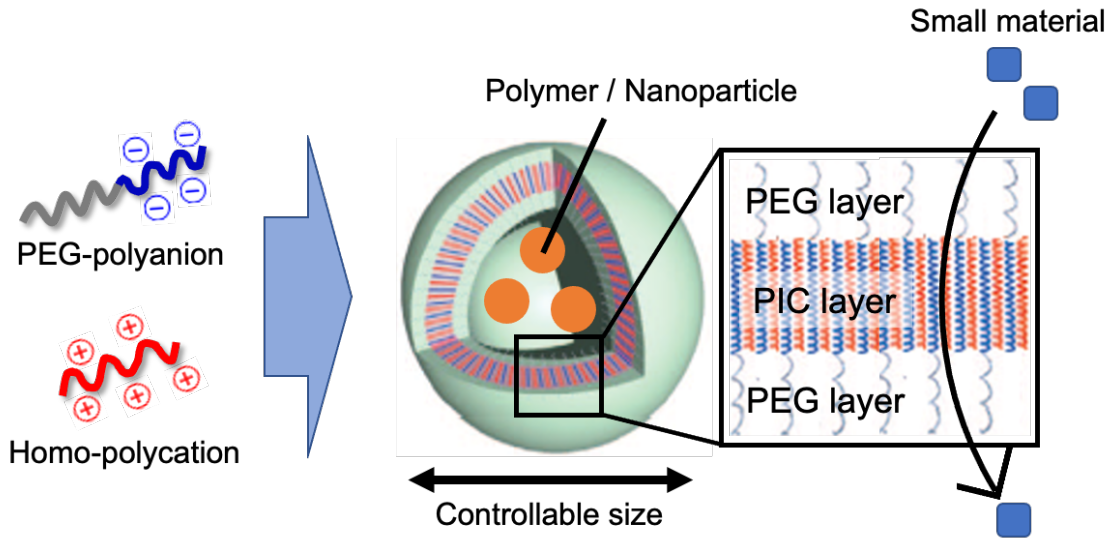

Figure 4. Structure of PICsome formed from PEG-polyanion and homo-polycation.

1-5. Research outline

In this study, hierarchization of PICsome was demonstrated in two ways; (i) PICsome multilamellarization and (ii) coacervate-in-PICsome formation in order to mimic the structure as well as the functionalities of mitochondria and nucleus, respectively (Figure 5). Multilamellar PICsome is expected to show efficient cascade reaction and/or segregation of incompatible molecules. Coacervate-in-PICsome is expected to show concentration of materials and/or molecular crowding. Both of hierarchical PIC structures can be considered to be a novel artificial organelle.

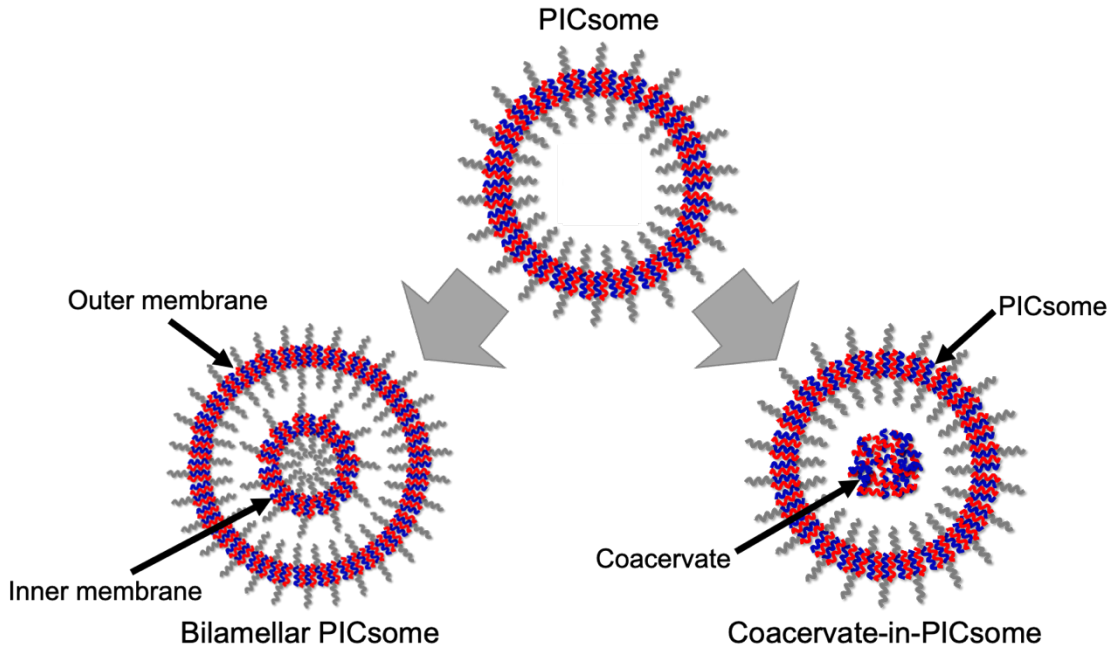

Figure 5. Hierarchization of PICsome by forming multilamellar PICsome and coacervate-in-PICsome.

Chapter 2 Multilamellarization of PICsome

2-1. Introduction

In this chapter, multilamellarization of PICsome was attempted by inducing shape transformation of unilamellar PICsome. As previously reported, vesicles formed via hydrophobic interaction such as liposome or polymersome can change their shape in response to osmotic stress [37-42]. Following to that, osmotic stress was introduced on PICsome membrane in order to induce inward budding of the membrane and form multilamellar structure (Figure 6). In addition to that, the transformation behavior of unilamellar PICsome into bilamellar structure was carefully examined from various perspectives.

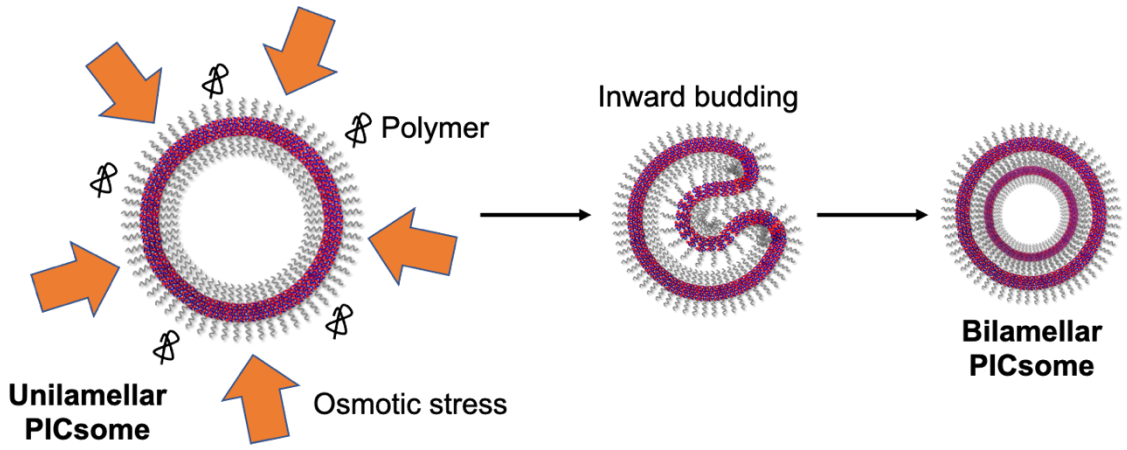

Figure 6. Schematic illustration of multilamellarization of PICsome under osmotic stress.

2-2. Experiments

2-2-1. Materials

Poly(ethylene glycol)-*b*-poly(α,β-aspartic acid) (PEG-PAsp; Mn of PEG = 2 kDa, degree of polymerization of PAsp = 93) was prepared as previously reported [25]. Poly-L-lysine (Homo-PLL; DP = 108) and dextran, from Leuconostoc spp. were purchased from Sigma-Aldrich Co. (St. Louis, MO, USA). 1-Ethyl-3-(3-dimethylaminopropyl)carbodiimide hydrochloride (EDC) was purchased from Tokyo Chemical Industry Co., Ltd. (Tokyo, Japan). Agarose S and ethanol were purchased from FUJIFILM Wako Pure Chemical Co. (Osaka, Japan). Quetol 812, DDSA, MNA and DMP30 were purchased from Nisshin EM Co., Ltd. (Tokyo, Japan). Sodium dihydrogen phosphate and disodium hydrogen phosphate were purchased from Nacalai Tesque Inc. (Kyoto, Japan).

2-2-2. Particle characterization

Dynamic light scattering (DLS) was conducted for size measurement by using a Zetasizer Nano ZS (Malvern Instruments, Malvern, UK). Particles were observed under fluorescence microscope or transmission electron microscope (TEM). Fluorescence microscope observation were performed by using BZ-X810 All-in-One fluorescence microscopy (Keyence, Osaka, Japan). For conventional TEM, particles were stained by 2% gadolinium acetate solution and observed by using JEM-2010 TEM (JEOL Ltd., Tokyo, Japan) at 120 kV. For cross-sectional TEM, particles were embedded in 3 wt% agarose and then gradually dehydrated with 50%~100% ethanol. After that, epoxy resin embedment was carried out (Quetol 810 45.5%, DDSA 31.0%, MNA 23.5%, DMP30 1.5%). Resin-embedded samples were sliced into 100 nm sections by using Ultracut UCT microtome (Leica Camera, Wetzlar, Germany). Fluorescence correlation spectroscopy (FCS) measurement was done to find the encapsulation of materials into the particles by using IX81 (Olympus Co., Tokyo, Japan). For FCS, samples were loaded into IBIDI slide and point FCS was carried out by 60X water immersion lens (NA > 0.22) at scan of 256. The in-built program 'Fluoview' was used to fit the curve after detrending with normalized Gaussian function as described below.

$$G(t) = \frac{1}{N}\left(1 + \frac{t}{\tau_D}\right)^{-1}\left(1 + \left(\frac{W_{xy}}{W_z}\right)2\,\frac{t}{\tau_D}\right)^{-\frac{1}{2}} \cdots (1)$$

$$\tau_D = \frac{W_{xy}^{\,2}}{4D} \cdots (2)$$

Where,

$W_o = W_{x,y} = 0.242786\ \mu m$

$W_z/W_o = 9.690274$ are confocal volume parameter calibrated by using standard Rhodamine dye

And,

$\langle N \rangle$ = Average number fluorescence particle in confocal volume

D = Translational diffusion coefficient

$G_o = 1/\langle N \rangle$ = Amplitude of autocorrelation function ($G(\tau)$ at $\tau = 0$)

τ_D is characteristic translational diffusion time

By measuring the decay curve of $G(\tau)$ as a function of time, the translational diffusion profile can be known and compared.

2-2-3. Preparation of PICsome and its bilamellarization

All the polymers used here were first dissolved in 10 mM phosphate buffer (PB) (pH 7.4) containing 150 mM NaCl at the concentration of 1 mg/mL. PEG_{2k}-PAsp and homo-PLL were mixed to fabricate PICsome via simple pipetting at cation/anion ratio (C/A) = 1 at 4 ℃. Then, Particles were incubated in water bath at 30 ℃ until the particle size reached ~400 nm. Once the particles with ~400 nm in size were obtained, they were immediately stored in refrigerator at 4 ℃ for o/n in order to suppress the particle growth. After confirming that the particle size did not change, 100 kDa dextran solution (final concentration: 20 x 10^{-5} mol/L) or 10 mM PB (as a control) were added into PICsome solution, followed by incubation at 4 ℃ for o/n. Particles were cross-linked by 100 mg/mL EDC (30 eq.) to stabilize the structure and purified by ultrafiltration using Vivaspin (MWCO = 300 kDa, Sartorius AG, Gottingen, Germany) for further analysis. For fluorescence microscope observation and FCS measurement, PEG_{2k}-PAsp was labelled with Cy3 via NHS coupling and 70 kDa dextran-FITC was used.

2-2-4. The effect of membrane flexibility

To investigate the effect of PICsome membrane flexibility on its bilamellarization, PICsome with ~400 nm in size was first cross-linked by EDC to stabilize the structure. Then, 100 kDa dextran was added into the solution of structure-stabilized PICsome at the final concentration of dextran is 20 × 10^{-5} mol/L. Morphology of the particles was observed under TEM. The particles without cross-linking were also prepared as a control at the same time.

2-2-5. The effect of dextran molecular weight

To investigate the effect of dextran molecular weight on PICsome bilamellarization, 100 kDa dextran, 10 kDa dextran and glucose were respectively added to the solution of PICsome with ~400 nm in size at the final concentration of dextran or glucose is 20 × 10^{-5} mol/L. Morphology of the particles was observed under TEM. The bilamellarization degree was calculated from obtained TEM images (n = 103 for 100 kDa dextran, n = 97 for 10 kDa dextran and n = 126 for glucose, where n is the counted number of particles for analysis).

$$\text{Bilamellarization degree (\%)} = \frac{\text{The number of bilamellar PICsome}}{\text{The total number of PICsome}} \times 100$$

2-2-6. The effect of PICsome size

To investigate the effect of PICsome size on its bilamellarization, PICsome with ~200 nm, ~300nm, ~400nm and ~500 nm in size were prepared by tuning the incubation time at the stage of particle growth as described earlier. Then, 100 kDa dextran was added to each of them at the final concentration of 1, 3, 5 and 10 × 10^{-5} mol/L. The bilamellarization degree was calculated in each sample.

2-2-7. The minimum particle size for bilamellarization

PICsome with ~300 nm in size was bilamellarized by the addition of 100 kDa dextran at the concentration of 1, 1.26, 1.6, 2, 3, 5, 7 and 10 × 10^{-5} mol/L and bilamellarization degree was calculated in each samples. Minimum particle size for bilamellarization was calculated from the histogram provided by DLS. In the histogram, the range of size which corresponded to the bilamellarization degree was exploited at each concentration of dextran and the median value of the size range was defined as minimum particle size for bilamellarization.

2-2-8. The inner/outer vesicle size ratio

From the TEM images obtained from the samples of PICsome size 400 nm and 500 nm, in which 1, 3, 5 and 10 × 10^{-5} mol/L of dextran were added, the inner and outer vesicle size of bilamellar PICsome were manually measured by using ruler. Inner vesicle size was plotted as a function of outer vesicle size and the ratio of inner vesicle size to outer vesicle size was calculated at each concentration of dextran. It should be noted that particles are assumed to be a squashed state in TEM images. Hence, the values of vesicle size were adjusted as shown in the figure below (Figure 7).

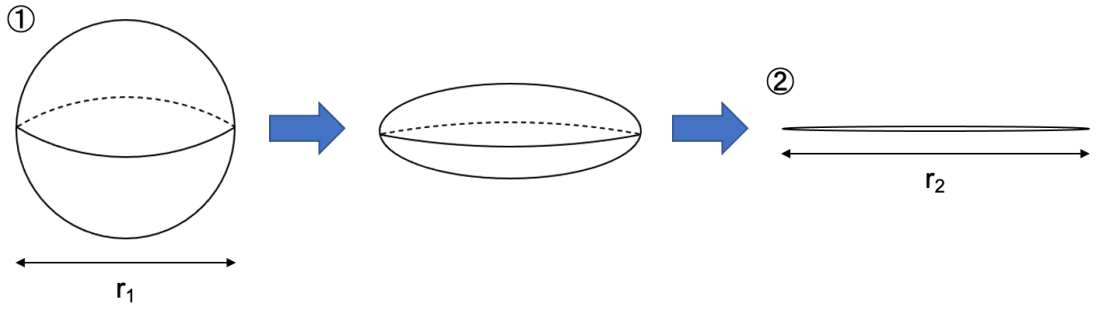

Surface area of sphere① = Area of circle② × 2

$$4 \times \pi \times r_1^2 = \pi \times r_2^2 \times 2$$

$$r_1 = 1/\sqrt{2} \times r_2$$

Figure 7. Calculation method of vesicle size from TEM images.

2-2-9. Multilamellarization of PICsome

To achieve the formation of multilamellar PICsome, the stepwise addition of dextran was attempted. First, 100 kDa dextran was added to the solution of PICsome with ~400 nm, where the final concentration of dextran was 5×10^{-5} mol/L. After incubation at 4 ℃ for o/n, another dose of 100 kDa dextran was added at the final concentration of 20×10^{-5} mol/L. In each step, the size and morphology of the particles were examined by DLS and TEM, respectively.

2-3. Results and discussion

2-3-1. Bilamellarization of PICsome

The reduction of particle size from ~400 nm to ~350 nm was confirmed by DLS measurement after the addition of dextran. On the other hand, the particle size was kept ~400 nm when PB was added as a control (Table 1). TEM and cross-sectional TEM images showed that PB-added particle maintained unilamellar structure but dextran-added particle was transformed into bilamellar structure (Figure 8). These results indicate that unilamellar PICsome transformed into bilamellar structure by inward budding of the membrane under osmotic stress.

Table 1. DLS results of PICsome before and after the addition of PB or dextran.

	Before	PB	Dextran
Size (d.nm)	399.7	410.5	345.7
PdI	0.136	0.151	0.183

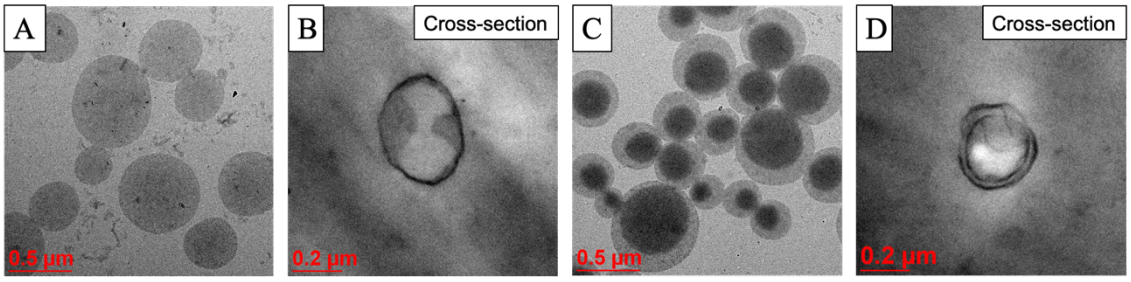

Figure 8. TEM (A, C) and cross-sectional TEM (B, D) images of unilamellar (A, B) and bilamellar (C, D) PICsome.

2-3-2. Dextran encapsulation

To verify that the mechanism of bilamellar PICsome formation is indeed membrane budding, the encapsulation of dextran in inner most layer was examined. From the result below, it is clear that the dextran added into PICsome solution had slower transitional motion compared to the free dextran and its function was overlapped with that of

PICsome (Figure 9A). This was also quantified as diffusion coefficient (Figure 9B). From this result, it can be considered that dextran was encapsulated into PICsome upon the bilamellarization, indicating that PICsome bilamellarization is derived from inward membrane budding.

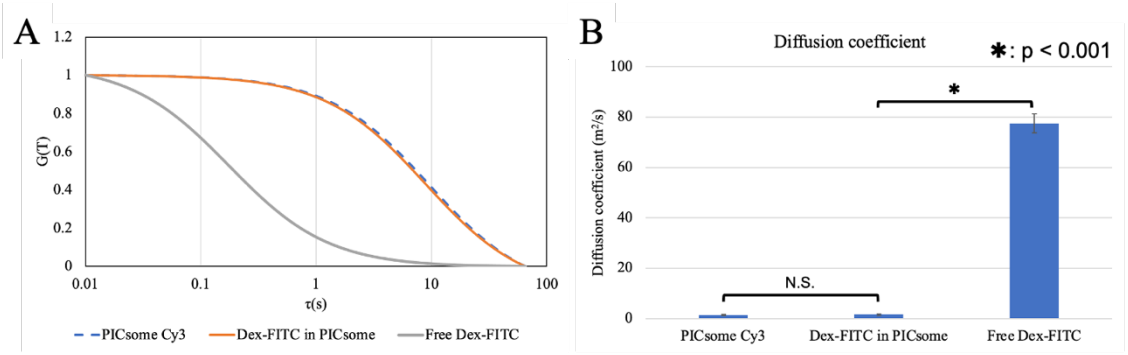

Figure 9. (A) Normalized autocorrelation function G(T) as a function of time τ(s) and (B) Diffusion coefficient of PICsome, dexran added into PICsome solution and free dextran.

Furthermore, fluorescent microscope images showed that PICsome and dextran were colocalized (Figure 10), which is in agreement with FCS result. The encapsulation efficiency of dextran was calculated to be as low as ~0.0462%, which indicates that the loading of molecules into bilamellar PICsome upon the membrane budding is a stochastic event without any attractive or repulsive interaction.

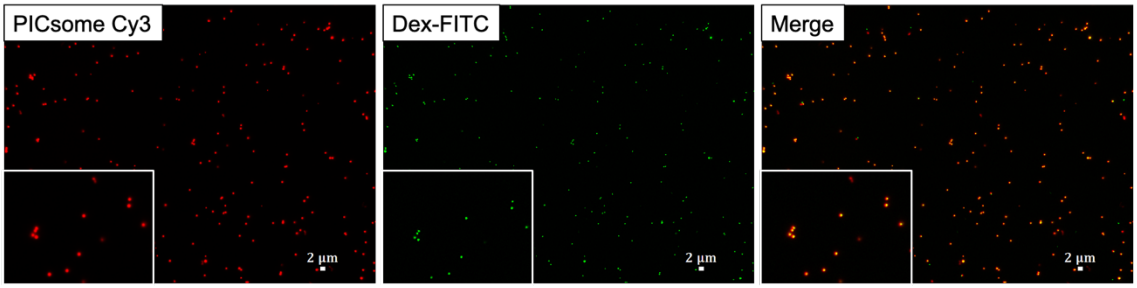

Figure 10. Fluorescent microscope images of bilamellar PICsome. Red: PICsome-Cy3, Green: Dex-FITC.

2-3-3. The effect of membrane flexibility

DLS measurement revealed that the size of cross-linked PICsome increased after the addition of dextran, which was different from non-cross-linked one (Table 2). It was confirmed that cross-linked PICsome maintained unilamellar structure even after the addition of dextran (Figure 11), indicating that high membrane flexibility is required for PICsome bilamellarization in two ways. First, the membrane cannot bud inward due to its high rigidity. Second, the edges of the membrane after inward budding cannot fuse each other to become complete bilamellar structure due to the restricted polymer mobility

inside membrane. As for the increased size after the addition of dextran in cross-linked PICsome, it can be considered that the sphericity of the particle is far from 1 due to partial buckling although it can maintain unilamellar structure.

Table 2. DLS results of PICsome with and without cross-linking before and after the addition of dextran.

	Before	Without cross-linking	With cross-linking
Size (d.nm)	374.3	319.1	504.8
PdI	0.144	0.170	0.193

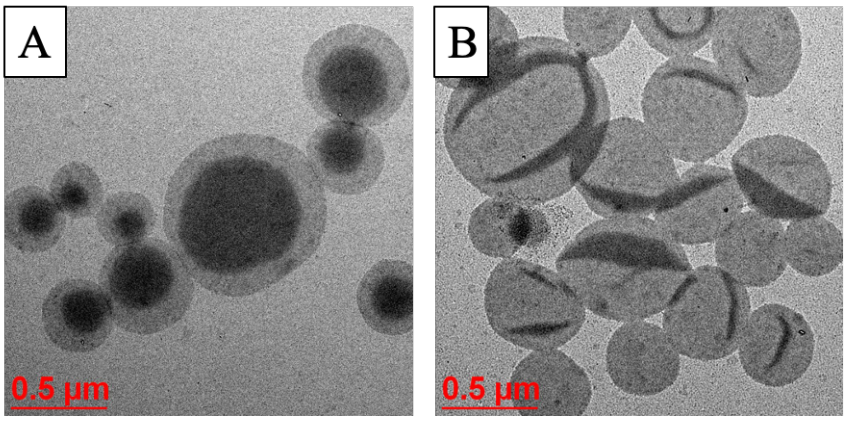

Figure 11. TEM images of (A) non-cross-linked and (B) cross-linked PICsome after the addition of dextran.

2-3-4. The effect of dextran molecular weight

By comparing the bilamellarization degree between each samples tested here, it was confirmed that the lower bilamellarization degree was, the lower the molecular weight of dextran was (Figure 12). This dependence on dextran molecular weight can be explained by semi-permeability of PICsome membrane. As previously reported, more than 40 kDa dextran cannot pass through PICsome membrane [27] and 10 kDa dextran gradually penetrate it [25]. Moreover, it is worth noting that 10 kDa dextran succeeded in bilamellarizing 80% of the particles. It can be considered that the speed of dextran permeation through PICsome membrane determines whether the particle transforms into bilamellar structure or not. Overall, this finding validated that high molecular weight of dextran is required for PICsome bilamellarization in order to produce osmotic imbalance across the membrane.

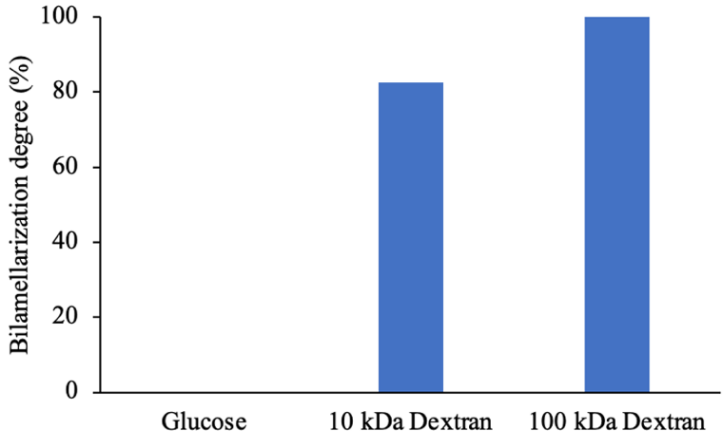

Figure 12. The effect of dextran molecular weight on the bilamellarization degree.

2-3-5. The effect of PICsome size

Comparison of bilamellarization degree between various sized particles with showed that the larger the particle size was, the higher the bilamellarization degree was at all dextran concentration (Figure 13), indicating that large particle can transform into bilamellar structure more easily than small one. This result is reasonable considering that large particle has large surface area and low curvature, both of which may be favorable for shape transformation under forces.

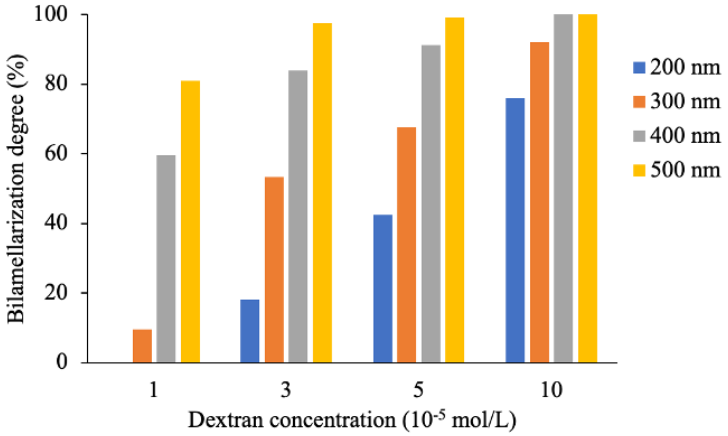

Figure 13. The effect of PICsome size on the bilamellarization degree.

2-3-6. The minimum particle size for bilamellarization

The histogram of PICsome with ~300 nm in size before bilamellarization and its bilamellarization degree plot as a function of dextran concentration is shown below (Figure 14).

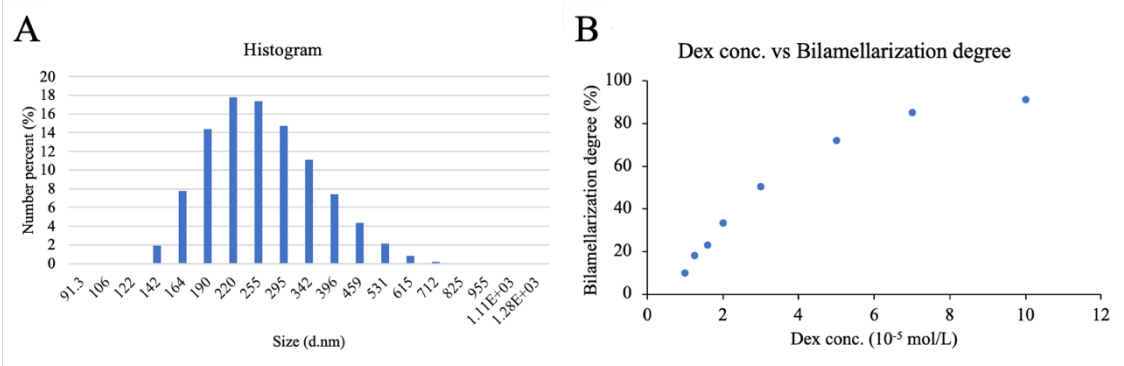

Figure 14. (A) Histogram of ~300 nm PICsome before bilamellarization. (B) Bilamellarization degree of ~300 nm PICsome as a function of dextran concentration.

Given that small particles are difficult to be bilamellarized as mentioned above, there should be a minimum particle size for bilamellarization at each concentration of dextran. The minimum particle size for bilamellarization was calculated as mentioned in the experiments section and plotted as a function of dextran concentration. As shown below, it was confirmed that the minimum for bilamellarization decreased with dextran concentration (Figure 15A), demonstrating that higher dextran concentration is necessary in order to bilamellarize smaller particles. To further analyze the relationship between PICsome size and dextran concentration, square of minimum particle size for bilamellarization was plotted as a function of reciprocal of dextran concentration. It was confirmed that that the square of minimum particle size for bilamellarization and the reciprocal of dextran concentration had a liner relationship (Figure 15B), which means that [square of minimum particle size for bilamellarization] x [dextran concentration] is constant. From this result, it can be considered that there is a threshold value of [particle surface area] x [osmotic pressure] for PICsome bilamellarization provided that square of particle size and dextran concentration are proportional to particle surface area and osmotic pressure, respectively.

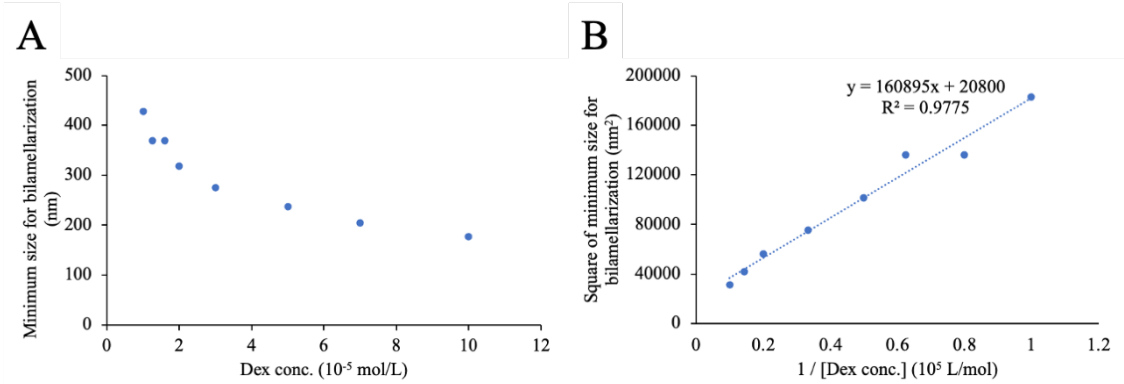

Figure 15. (A) Minimum particle size for bilamellarization plot over dextran concentration and (B) square of minimum particle size for bilamellarization plot over reciprocal of dextran concentration.

2-3-7. The inner/outer vesicle size ratio

To characterize the morphological property of bilamellar PICsome, the inner and outer vesicle size was measured. The inner vesicle size vs outer vesicle size plot at various concentrations of dextran showed that inner vesicle size was linearly correlated with outer vesicle size at all concentration of dextran, indicating that the ratio of inner vesicle size to outer vesicle size is independent on PICsome size (Figure 16A-D). Moreover, it was also revealed that the ratio of inner vesicle size to outer vesicle size was constantly ~0.8 independent on dextran concentration (Figure 16E). These results demonstrated that both PICsome size and dextran concentration is not involved in the determination of inner and outer vesicle size. Hence, it can be considered that changing membrane properties such as elasticity are required in order to modulate inner and outer vesicle size of bilamellar PICsome.

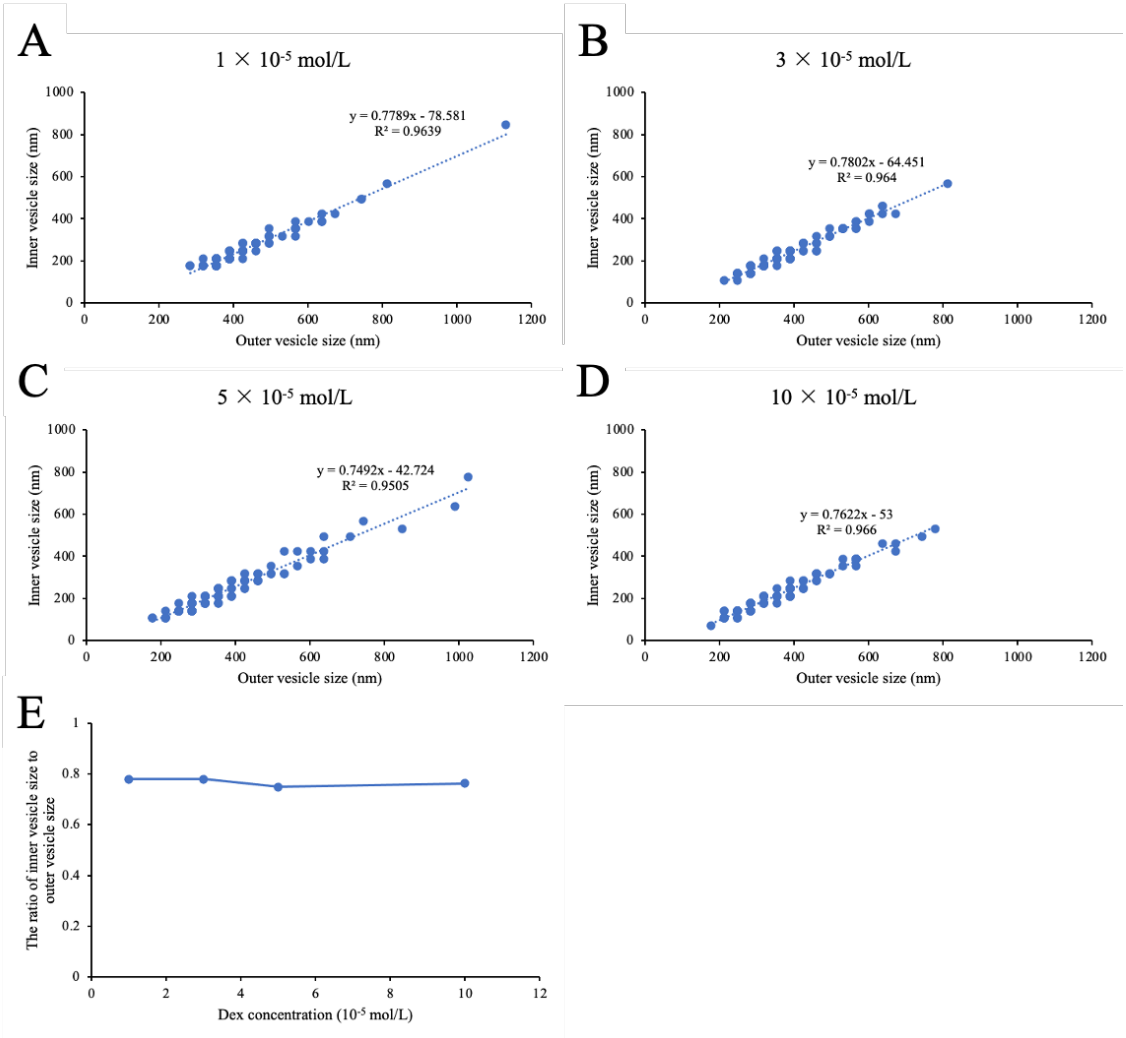

Figure 16. (A-D) Inner vesicle size vs outer vesicle size plot at dextran concentration of 1 x 10^{-5} mol/L (A), 3 x 10^{-5} mol/L (B), 5 x 10^{-5} mol/L (C) and 10 x 10^{-5} mol/L (D). (E) The ratio of inner vesicle size to outer vesicle size plot over dextran concentration.

Furthermore, the change of inner vesicle volume upon the bilamellarization, defined as V'/V, where V is the original vesicle volume and V' is the final vesicle volume after bilamellarization was calculated by utilizing the ratio of inner vesicle size to outer vesicle size obtained above (Figure 17). It can be assumed that the surface area (A) does not change upon the bilamellarization considering the mechanism of shape transformation. V' and A can be described by the formula (1) and (2), respectively as shown below.

$$V' = \frac{4}{3}\pi (r_1^3 - r_2^3) \quad (1)$$

$$A = 4\pi (r_1^2 + r_2^2) \quad (2)$$

Provided that r_2/r_1 is 4/5 as calculated above, (1) and (2) are expressed like

$$V' = \frac{244}{375}\pi r_1^3 \quad (3)$$

$$A = \frac{164}{25}\pi r_1^2 \quad (4)$$

Considering the relationship between V and A, V can be represented as

$$V = \frac{1}{3}(4\pi)^{-\frac{1}{2}} A^{\frac{3}{2}} \quad (5)$$

From equation (3) to (5), V'/V is written as

$$\frac{V'}{V} = 3\ (4\pi)^{\frac{1}{2}} \frac{V'}{A^{\frac{3}{2}}} = \frac{122}{125\pi} \left(\frac{164}{25}\right)^{-\frac{3}{2}} \approx 0.232$$

Hence, it was confirmed that ~80% of the initial vesicle volume was reduced upon bilamellarization, which is in agreement with previous theoretical study [43]. This finding indicates that water molecules efflux out of vesicle due to osmotic imbalance across the membrane, leading to membrane budding.

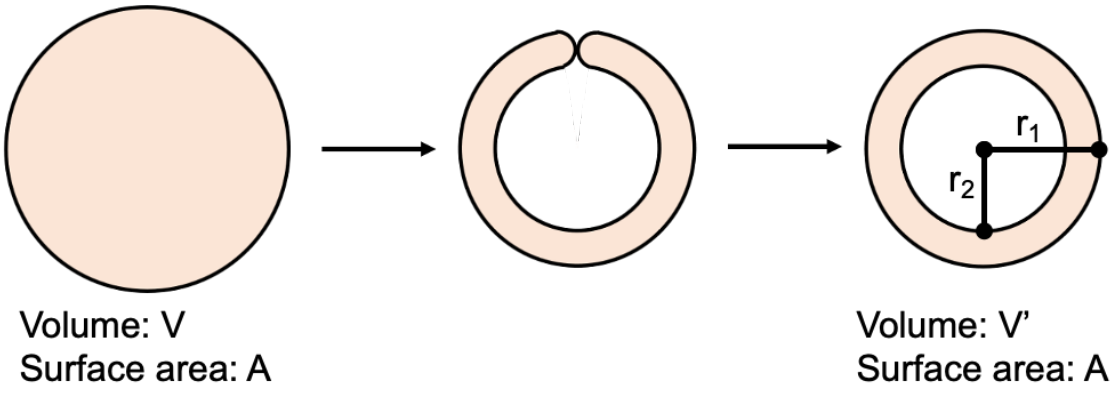

Figure 17. Schematic illustration of bilamellarization process.

2-3-8. Multilamellarization of PICsome

Sequential introduction of osmotic stress onto PICsome membrane was attempted in order to induce further shape transformation from bilamellar to multilamellar structure. To this end, low concentration of dextran (final concentration: 5 x 10^{-5} mol/L) and high concentration of dextran (final concentration: 20 x 10^{-5} mol/L) was added to PICsome solution in a row. The size reduction was confirmed at each steps of dextran addition by DLS measurement, which was consistent with the results described earlier (Table 3). TEM and cross-sectional TEM images showed that PICsome with ~400 nm in original size which became bilamellar structure at low dextran concentration further transformed into multilamellar structure after the addition of high concentration of dextran (Figure 18). It should be noted that tetralamellar structure was supposed to be formed after two-step addition of dextran considering the transformation mechanism. The unexpected formation of hexalamellar structure may be attributed to the concentration variations between each layer, leading to further budding of inner two membranes after the formation of tetralamellar structure even though osmotic stress was not applied anymore.

Table 3. DLS results of PICsome before and after the addition of low and high concentration of dextran.

	Before	Low	High
Size (d.nm)	402.2	351.5	287.6
PdI	0.071	0.093	0.109

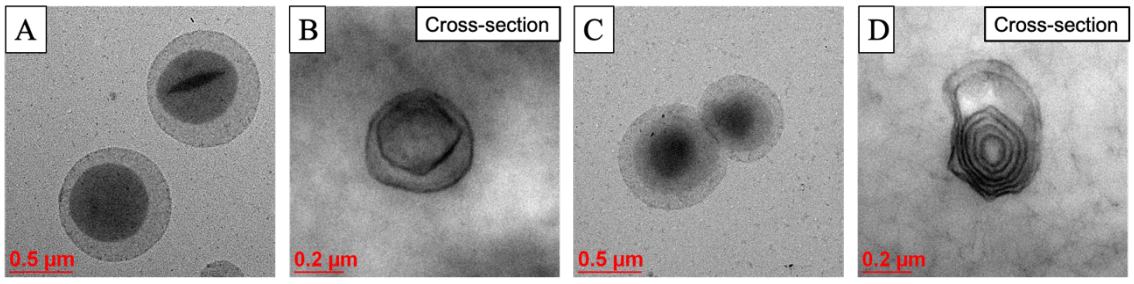

Figure 18. TEM (A, C) and cross-sectional TEM (B, D) images of bilamellar (A, B) and multilamellar (C, D) PICsome.

2-4. Conclusion of this chapter

In this chapter, bilamellarization of PICsome was achieved by introducing osmotic stress onto PICsome with high concentration of dextran as an osmotic stress inducer, in which inward budding of the membrane might take place. For further investigation, the relevant factors to PICsome bilamellarization such as membrane flexibility, dextran molecular weight and PICsome size as well as the morphological property of bilamellar

PICsome; inner/outer vesicle size ratio were clarified. Finally, multilamellarization of PICsome was demonstrated by sequentially introducing osmotic stress.

Chapter 3 Coacervate-in-PICsome formation

3-1. Introduction

In this chapter, formation of coacervate-in-PICsome was explored by simultaneously mixing PICsome components and coacervate components. To this end, PEG-polyanion, homo-polyanion and homo-polycation were mixed, in which PEG-polyanion/homo-PLL forms PICsome and homo-PAsp/homo-PLL forms coacervate, respectively (Figure 19). Especially, the effect of polymer interaction strength between PICsome components and coacervate components was extensively studied by tuning the charge density in homo-polyanion, which can lead to the elucidation of formation mechanism of coacervate-in-PICsome.

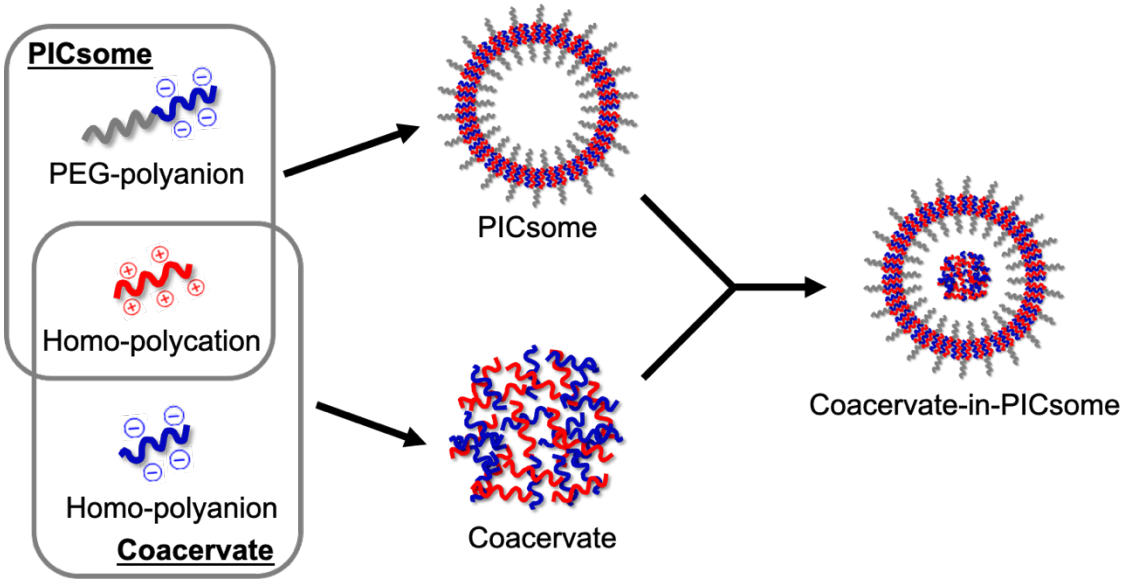

Figure 19. Schematic illustration of coacervate-in-PICsome formation by integrating them.

3-2. Experiments

3-2-1. Materials

PEG_{2k}-$PAsp_{67}$, PEG_{5k}-$PAsp_{67}$, homo-$PAsp_{107}$, homo-$PAsp_{28}$-OH_{56}, homo-$PAsp_{45}$-$(CH_3)_{39}$ and PEG_{2k}-$PAsp_{46}$-OH_{27} were prepared as previously reported [25]. Homo-PLL_{108} was purchased from Sigma-Aldrich Co. (St. Louis, MO, USA). 1-Ethyl-3-(3-dimethylaminopropyl)carbodiimide hydrochloride (EDC) was purchased from Tokyo Chemical Industry Co., Ltd. (Tokyo, Japan). Agarose S, ethanol and glutaraldehyde (GA) were purchased from FUJIFILM Wako Pure Chemical Co. (Osaka, Japan). Quetol 812, DDSA, MNA and DMP30 were purchased from Nisshin EM Co., Ltd. (Tokyo, Japan). Sodium dihydrogen phosphate and disodium hydrogen phosphate were purchased from Nacalai Tesque Inc. (Kyoto, Japan).

3-2-2. Preparation of coacervate-in-PICsome

All the polymers used here were first dissolved in 10 mM phosphate buffer (pH 7.4) at the concentration of 1 mg/mL. Two polyanions were pre-mixed at specific Coa/PIC (The ratio of charge number between PICsome component and coacervate component), followed by the addition of polycation at cation/anion ratio (C/A) = 1. Particles were cross-linked by 100 mg/mL EDC (30 eq.) or 25% GA (50 eq.) to stabilize the structure and purified by ultrafiltration using Vivaspin (MWCO = 300 kDa, Sartorius AG, Gottingen, Germany) or sedimentation and supernatant exchange for further analysis.

3-2-3. Particle characterization

Dynamic light scattering (DLS) was conducted for size measurement by using a Zetasizer Nano ZS (Malvern Instruments, Malvern, UK). The morphology of the particles was observed under optical microscope, fluorescence microscope or transmission electron microscope (TEM). Optical microscope and fluorescence microscope observation were performed by using BZ-X810 All-in-One fluorescence microscopy (Keyence, Osaka, Japan). For TEM, particles were stained by 2% gadolinium acetate solution and observed by using JEM-2010 TEM (JEOL Ltd., Tokyo, Japan) at 120 kV. For cross-sectional TEM, particles were embedded in 3 wt% agarose and then gradually dehydrated with 50%~100% ethanol. After that, epoxy resin embedment was carried out (Quetol 810 45.5%, DDSA 31.0%, MNA 23.5%, DMP30 1.5%). Resin-embedded samples were sliced into 100 nm sections by using Ultracut UCT microtome (Leica Camera, Wetzlar, Germany).

3-3. Results and discussion

3-3-1. Complexation with Homo-PAsp

Polymer combination of PEG-PAsp/homo-PAsp/homo-PLL was first examined. Given that charged block in PEG-PAsp and homo-PAsp have the same charge density, PICsome components and coacervate components can be considered to have the same polymer interaction strength. After mixing these polymers at C/A = 1 and Coa/PIC = 1, the solution was transparent, indicating that any micron-sized particles or aggregates did not form. DLS measurement revealed that mono-dispersed particle with ~300 nm in size was formed (Table 4). Considering that PICsome formed from PEG-PAsp/homo-PLL is ~100 nm in size and coacervate formed from homo-PAsp/homo-PLL is > 1 μm, the size of this particle seems to be reasonable. TEM and cross-sectional TEM observation confirmed the formation of multicompartment micelle, which is composed of PIC continuous phase and a number of water phases (Figure 20) although coacvervate-in-PICsome was not

formed in this condition. This result indicates that PICsome components and coacervate components mix equally in the complex and formed homogenous particle, based on the same polymer interaction strength between PICsome components and coacervate components.

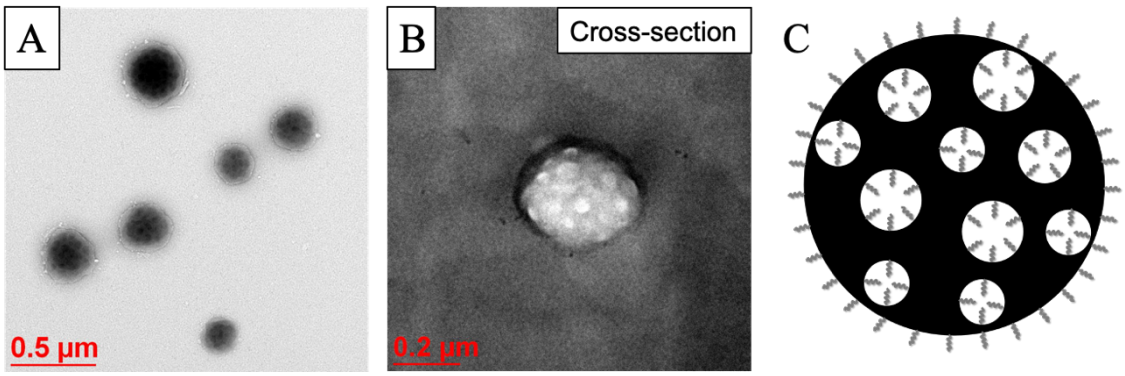

Figure 20. (A) TEM image, (B) cross-sectional TEM image and (C) illustration of multicompartment micelle.

In addition, the effect of mixing ratio between PICsome components and coacervate components on the multicompartment micelle formation was investigated. For that purpose, Coa/PIC was varied from 0.5 up to 10. In all cases tested here, similar structures with above mentioned sample was confirmed, of which size range from 200 nm to 500 nm (Figure 21 and table 4). Moreover, comparison between cross-sectional TEM images of the samples at Coa/PIC = 0.5, 1, 4 revealed that the volume ratio of PIC phase to water phase in the multicompartment micelle increased as Coa/PIC increased (Figure 21). This result is consistent with the hypothesis that the formation of multicompartment micelle is attributed to the same polymer interaction strength between PICsome components and coacervate components.

Table 4. DLS results of multicompartment micelles formed at various Coa/PIC.

Coa/PIC	0.5	1	2	4	6	8	10
Size (d.nm)	362.8	271.7	226.4	247.7	273.3	338.8	459.8
PdI	0.115	0.090	0.047	0.083	0.043	0.074	0.0460

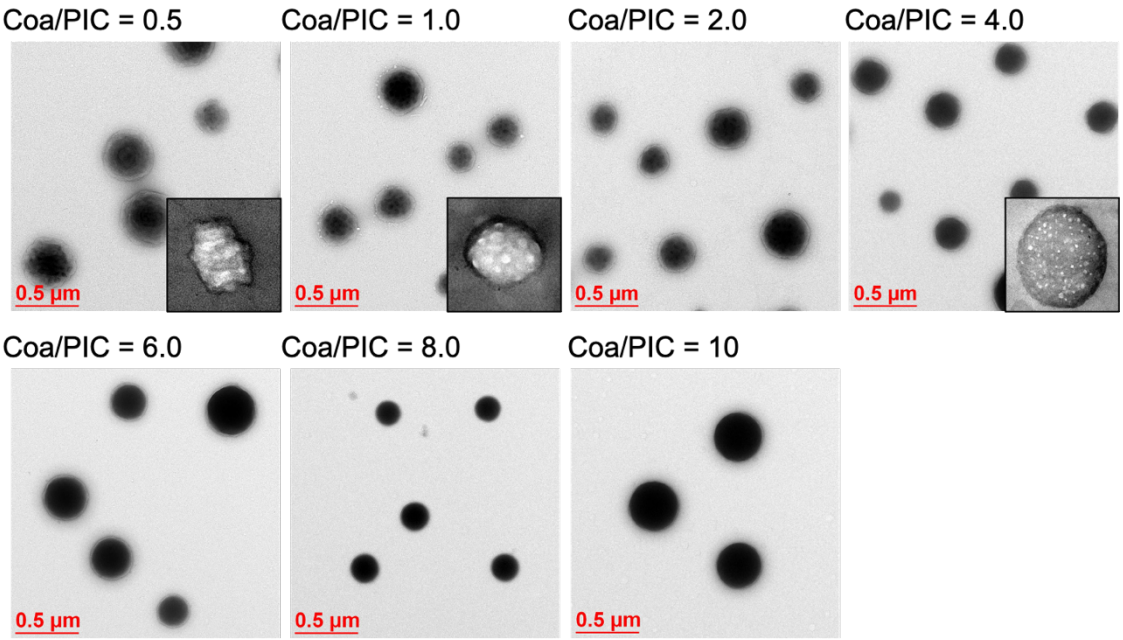

Figure 11. TEM images of multicompartment micelles formed at various Coa/PIC.

3-3-2. Phase separation hypothesis

As mentioned above, PICsome components and coacervate components homogenously mixed in the complex when they have the same polymer interaction strength. Hence, it can be hypothesized that phase separation between PICsome and coacervate is required for the formation of coacervate-in-PICsome (Figure 22). Phase separation between two or more coacervates, known as multiphase coacervation has been recently reported [44-46]. It has been said that multiphase coacervation takes place if the polymer interaction strength between each coacervate components is significantly different, for example by differentiating the charge density between them [45]. Therefore, phase separation between PICsome and coacervate was implemented by differentiating the polymer interaction strength between them.

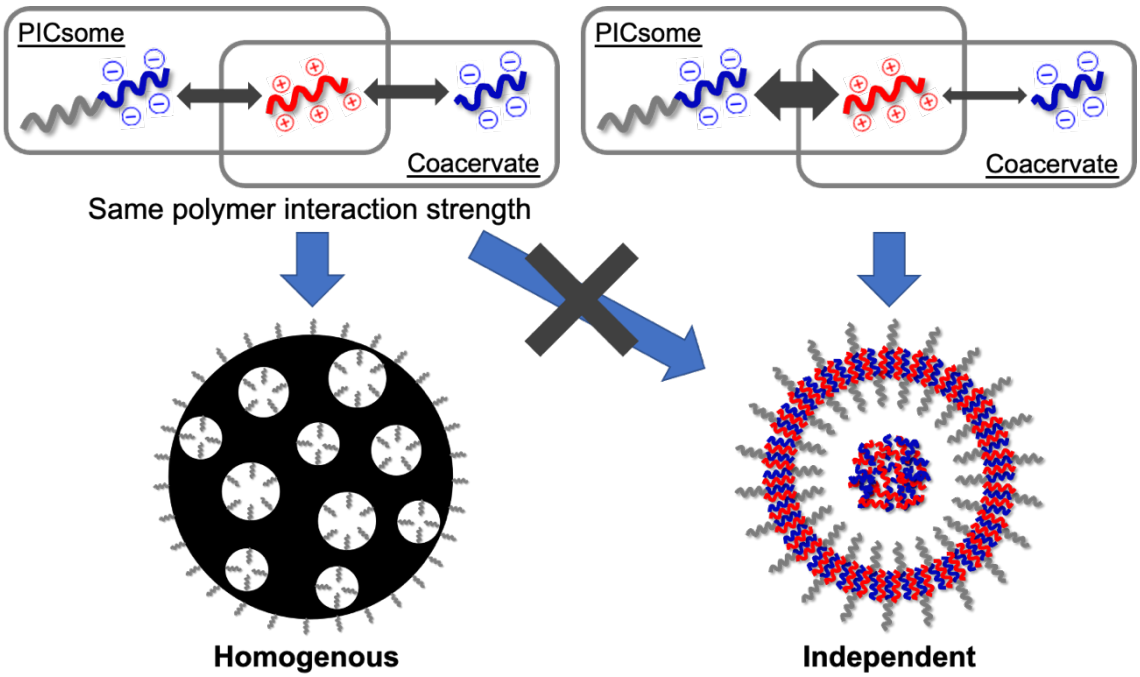

Figure 22. Schematic illustration of phase separation hypothesis for coacervate-in-PICsome formation.

3-3-3. Complexation with Homo-PAsp-OH

To differentiate the polymer interaction strength between PICsome component and coacervate component, the side-chain of homo-PAsp was randomly modified with hydroxyl group to decrease its charge density, leading to the decrease of polymer interaction strength in coacervate components. After mixing the polymers of PEG-PAsp/homo-PAsp-OH/homo-PLL, the solution became turbid, indicating the formation of micron-sized particle. Strikingly, the formation of nested multiphase coacervate, in which one coacervate was encapsulated in another coacervate was confirmed under optical microscope (Figure 23A). Furthermore, cross-sectional TEM observation revealed that this nested multiphase coacervate had microphase separated structure, which is composed of PIC domain and PEG domain based on their immiscibility [47] only in the outer phase (Figure 23B,C). It can be considered that the difference of charge density between charged block in PEG-PAsp and homo-PAsp-OH induced multiphase separation, which is consistent with the previous report [45]. Considering that only outer phase contained microphase separated structure, outer phase and inner phase seem to be mainly composed of PEG-PAsp and homo-PAsp-OH, respectively.

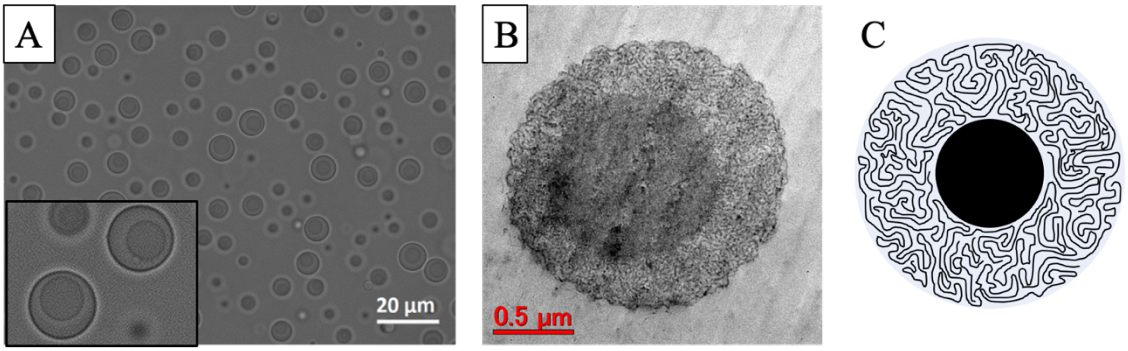

Figure 23. (A) Optical microscope image, (B) cross-sectional TEM image and (C) illustration of nested multiphase coacervate by homo-PAsp-OH.

Next, the effect of mixing ratio between PICsome components and coacervate components on the formation of nested multiphase coacervate was explored by varying Coa/PIC from 0.5 to 2.0. It was confirmed that foam-like structure was formed at Coa/PIC = 0.5 under optical microscope (Figure 24). Also, the volume ratio of inner phase increased as Coa/PIC increased, finally resulting in homogenous one phase coacervate. From this result, it can be considered that if the mixing ratio between PICsome components and coacervate components is far from their equivalence, phase separation cannot take place and mix homogenously.

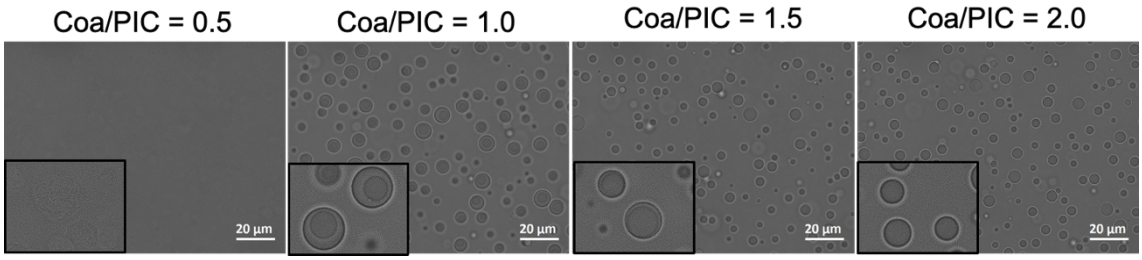

Figure 24. Optical microscope images of complexes formed from PEG-PAsp/homo-PAsp-OH/homo-PLL at various Coa/PIC.

To investigate the effect of the kind of polymer which has low charge density on multiphase coacervation, PEG-PAsp was modified with hydroxyl group to decrease it charge density instead of homo-PAsp. It was revealed that the polymer combination of PEG-PAsp-OH/homo-PAsp/homo-PLL formed tethered multiphase coacervate, in which a number of coacervates were attached on one coacervate under optical microscope (Figure 25A). Moreover, cross-sectional TEM observation revealed that the center coacervate contained microphase separated structure but surrounding ones did not (Figure 25B,C), which indicates that the former is mainly composed of PEG-PAsp-OH and the latter is mainly composed of homo-PAsp.

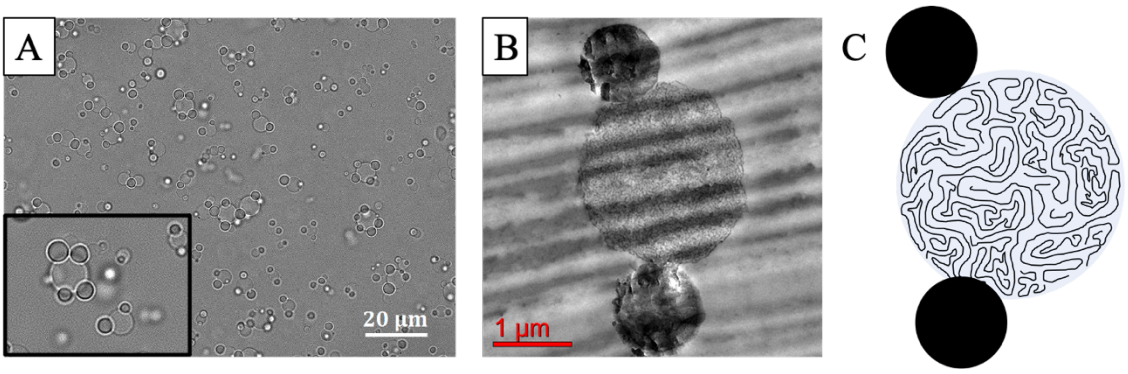

Figure 25. (A) Optical microscope image, (B) cross-sectional TEM image and (C) illustration of tethered multiphase coacervate.

As shown in the figure below, each coacervate in nested and tethered multiphase coacervate was named coacervate 1 to 4 for the ease of discussion (Figure 26). Then, the relationship of interfacial tension in each coacervate is represented as $\gamma_1 + \gamma_{12} < \gamma_2$ in nested type and $\gamma_3 < \gamma_{34}$ and $\gamma_4 < \gamma_{34}$ in tethered type according to the previous reports [45]. The difference of their interfacial tension, especially between γ_{12} and γ_{34} may be attributed that the difference of polymer nature between PEG-PAsp-OH and homo-PAsp is significantly large compared with that between PEG-PAsp and homo-PAsp-OH, leading to relatively low interfacial tension between coacervate 1 and 2 and relatively high interfacial tension between coacervate 3 and 4.

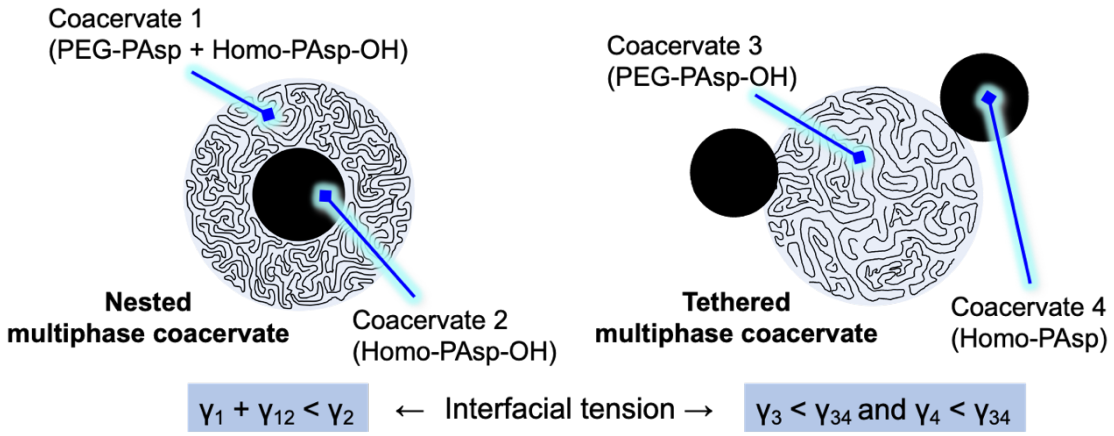

Figure 26. Comparison between nested and tethered multiphase coacervate with respect to their interfacial tension.

3-3-4. Complexation with Homo-PAsp-CH_3

In the polymer combination of PEG-PAsp/homo-PAsp-OH/homo-PLL, the fact that vesicle structure was not formed indicates that homo-PAsp-OH also participated in and interrupted the formation of vesicle structure. In order to avoid it, homo-PAsp was modified with methyl group, which is more hydrophobic than hydroxyl group to enhance

the self-interaction strength of coacervate component to promote phase separation into PICsome and coacervate. However, the polymer combination of PEG-PAsp/homo-PAsp-CH_3/homo-PLL formed nested multiphase coacervate similar with homo-PAsp-OH case (Figure 27). It can be considered that self-interaction strength of coacervate component was not enough to prevent homo-PAsp-CH_3 from interrupt PICsome formation. Hence, exploiting the polymer with stronger self-interaction strength or high steric hindrance such as longer chain, dendrimer, etc. as coacervate component can be considered promising for forming PICsome and coacervate simultaneously.

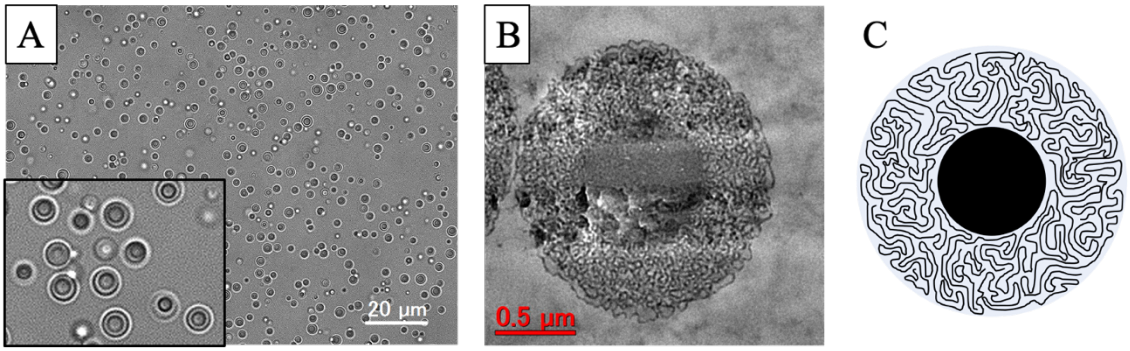

Figure 27. (A) Optical microscope image, (B) cross-sectional TEM image and (C) illustration of nested multiphase coacervate by homo-PAsp-CH_3.

3-3-5. Lamellar structure hypothesis

Given that only outer coacervate contained microphase separated structure in the nested multiphase coacervate, it can be considered that coacervate-in-PICsome formation can be achieved if outer phase become vesicle structure while maintaining inner coacervate as shown in the below (Figure 28). Considering the PEG fraction in this system, the microphase separated structure of the outer phase in the nested multiphase coacervate might correspond to PEG-gyroid structure. Therefore, it can be hypothesized that increasing PEG fraction into the range of lamellar structure induce vesicle formation on behalf of outer coacervate, leading to coacervate-in-PICsome formation.

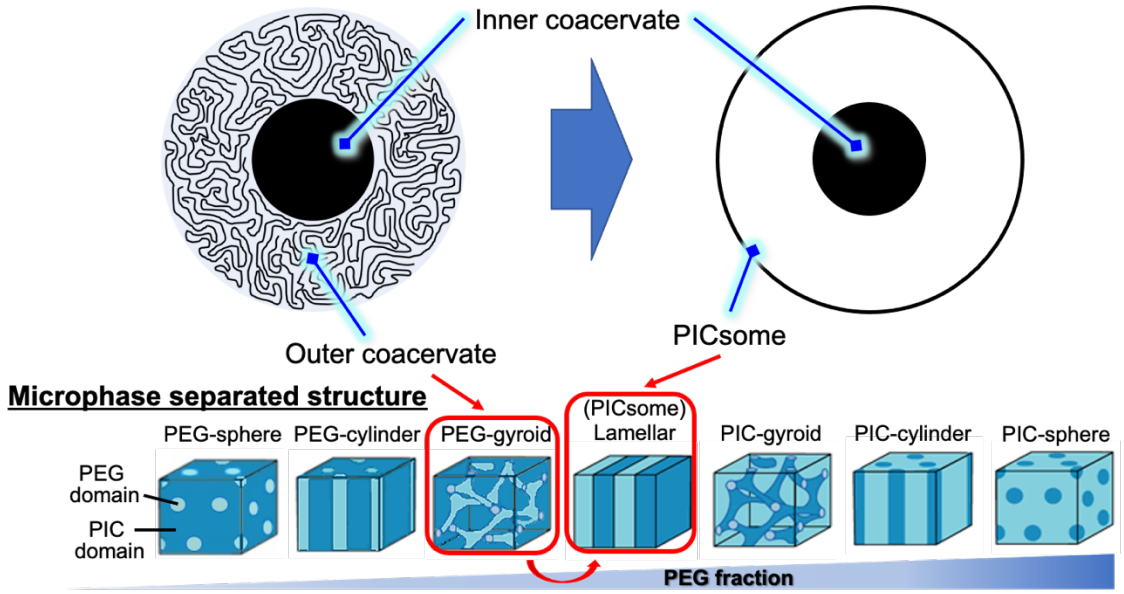

Figure 28. Schematic illustration of vesicle induction from outer coacervate in nested multiphase coacervate.

3-3-6. Vesicle induction by tuning PEG fraction

To increase the PEG fraction, PEG_{5k}-PAsp was added at f_{5k} = 0.2 in the polymer combination of PEG-PAsp/homo-PAsp-CH_3/homo-PLL. Fluorescent microscope, TEM and cross-sectional TEM images showed that coacervate-in-PICsome was successfully formed (Figure 29). Although some of the particles were still incomplete coacervate-in-PICsome such as flower-like shape due to the complexity of quaternary polymer system, vesicle induction from outer coacervate while keeping inner coacervate intact was demonstrated. From these findings, it can be considered that (i) PICsome and coacervate should phase separate based on the difference of their polymer interaction strength between and (ii) PICsome components should maintain the capability of forming lamellar structure.

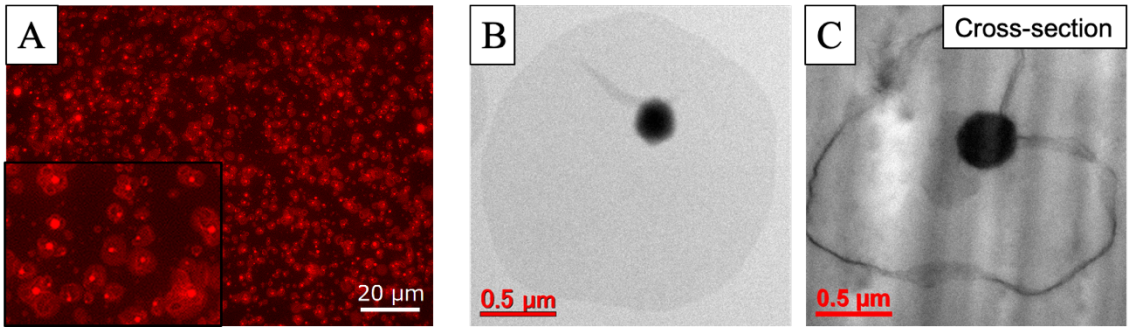

Figure 29. (A) Fluorescent microscope, (B) TEM and (C) cross-sectional TEM images of coacervate-in-PICsome.

3-4. Conclusion of this chapter

In this chapter, ternary polymer combination of PEG-polyanion, homo-polyanion and homo-polycation was mixed together to form coacervate-in-PICsome. On the way to the goal, multiphase coacervate with microphase separated structure was accidentally formed. In addition, it was revealed that two types of multiphase coacervates; nested and tethered could be formed by modulating polymer characteristics and polymer combination. Formation of coacervate-in-PICsome was finally achieved by tuning the microphase separated structure in nested multiphase coacervate.

Chapter 4 Conclusion and future perspective

4-1 Conclusion

In order to create an artificial organelle with hierarchical structure based on bottom-up approach, PIC system was exploited due to its capability of forming a wide variety of structures, which is expected to enable the hierarchization of the structure by fine-tuning the environmental condition or polymer characteristics. In this study, two types of novel hierarchical PIC structures were formed; multilamellar PICsome and coacervate-in-PICsome.

Multilamellarization of PICsome was demonstrated by inducing the shape transformation under osmotic stress. The further investigation on the relevant factors to PICsome bilamellarization highlights that flexible membrane, high molecular weight dextran and large size of PICsome are favorable for its transformation into bilamellar structure. Moreover, the fact that inner/outer vesicle size ratio is independent on PICsome size and dextran concentration indicates that tuning other factors such as membrane flexibility or temperature is required for controlling the inner/outer vesicle size ratio of bilamellar PICsome.

Formation of coacervate-in-PICsome was attempted by mixing PICsome components and coacervate components and tuning polymer characteristics. The obtained results indicate that in order to form coacervate-in-PICsome, (i) phase separation into PICsome and coacervate and (ii) maintenance of membrane-forming ability in PICsome components are important prerequisites. Furthermore, formation of nested and tethered multiphase coacervate with microphase separated structure were achieved by using PEG-based polyanion and homo-polyanion, one of which was modified with neutral groups to decrease the charge density.

The results and insights obtained in this work provide a promising strategy to create a wide variety of hierarchical structures based on PIC system.

4-2 Future perspective

Two types of hierarchical PIC structures were successfully fabricated by tuning environmental condition or polymer characteristics. In terms of structural control based on PIC formation, some fruitful insights have been collected although other hierarchical structures can be expected more such as multilamellar multiphase coacervate-in-PICsome or multiphase coacervate with a variety of microphase separated structures. Therefore, functionalization of the hierarchical PIC structures will be the next step toward creating artificial organelles. One way of endowing them more life-like behavior is to make it non-

equilibrium system. For example, reversible formation and dissociation of inner vesicle or coacervate while surrounding vesicle is intact in response to external stimuli. Implementation of biochemical reactions inside hierarchical PIC structures is also intriguing, especially including two or more steps of cascade reactions. In the future, it can be expected that these artificial organelles with hierarchical structures and highly organized functions are able to communicate with each other to further constitute artificial cells and tissues.

References

[1] Courchaine, E. M., Lu, A. & Neugebauer, K. M. Droplet organelles? *EMBO J.* **35**, 1603–1612 (2016).

[2] Giacomello, M., Pyakurel, A., Glytsou, C. & Scorrano, L. The cell biology of mitochondrial membrane dynamics. *Nat. Rev. Mol. Cell Biol.* **21**, 204–224 (2020).

[3] Zhang, H. & Hu, J. Shaping the Endoplasmic Reticulum into a Social Network. *Trends Cell Biol.* **26**, 934–943 (2016).

[4] Tao, Y., Yang, Y., Zhou, R. & Gong, T. Golgi Apparatus : An Emerging Platform for Innate Immunity. *Trends Cell Biol.* **30**, 467–477 (2020).

[5] Damiati, S. New opportunities for creating man-made bioarchitectures utilizing microfluidics. *Biomed. Microdevices* **21**, (2019).

[6] Vieregg, J. R. & Tang, T. Y. D. Polynucleotides in cellular mimics: Coacervates and lipid vesicles. Curr. Opin. *Colloid Interface Sci.* **26**, 50–57 (2016).

[7] Martin, N. & Douliez, J. Fatty Acid Vesicles and Coacervates as Model Prebiotic Protocells. *ChemSystemsChem* **3**, (2021).

[8] Einfalt, T. et al. Biomimetic artificial organelles with in vitro and in vivo activity triggered by reduction in microenvironment. *Nat. Commun.* **9**, 1–12 (2018).

[9] Wanzke, C. et al. Dynamic Vesicles Formed By Dissipative Self-Assembly. *ChemSystemsChem* **2**, 1–7 (2020).

[10] Gonzales, D. T., Yandrapalli, N., Robinson, T., Zechner, C. & Tang, T. Y. D. Cell-Free Gene Expression Dynamics in Synthetic Cell Populations. *ACS Synth. Biol.* **11**, 205–215 (2022).

[11] Martin, N. et al. Photoswitchable Phase Separation and Oligonucleotide Trafficking in DNA Coacervate Microdroplets. *Angew. Chemie* **131**, 14736–14740 (2019).

[12] Nakashima, K. K., Baaij, J. F. & Spruijt, E. Reversible generation of coacervate droplets in an enzymatic network. *Soft Matter* **14**, 361–367 (2018).

[13] Donau, C. et al. Active coacervate droplets as a model for membraneless organelles and protocells. *Nat. Commun.* **11**, 1–10 (2020).

[14] Iglesias-Artola, J. M. et al. Charge-density reduction promotes ribozyme activity in RNA–peptide coacervates via RNA fluidization and magnesium partitioning. *Nat. Chem.* (2022).

[15] Späth, F. et al. Molecular Design of Chemically Fueled Peptide-Polyelectrolyte Coacervate-Based Assemblies. *J. Am. Chem. Soc.* **143**, 4782–4789 (2021).

[16] Martin, N., Li, M. & Mann, S. Selective Uptake and Refolding of Globular Proteins in Coacervate Microdroplets. *Langmuir* **32**, 5881–5889 (2016).

[17] Nolles, A. et al. Encapsulation of GFP in complex coacervate core micelles. *Biomacromolecules* **16**, 1542–1549 (2015).
[18] Drogoz, A., David, L., Rochas, C., Domard, A. & Delair, T. Polyelectrolyte complexes from polysaccharides: Formation and stoichiometry monitoring. *Langmuir* **23**, 10950–10958 (2007).
[19] Kim, B. S. et al. Self-Assembly of siRNA/PEG- b-Catiomer at Integer Molar Ratio into 100 nm-Sized Vesicular Polyion Complexes (siRNAsomes) for RNAi and Codelivery of Cargo Macromolecules. *J. Am. Chem. Soc.* **141**, 3699–3709 (2019).
[20] Obermeyer, A. C., Mills, C. E., Dong, X. H., Flores, R. J. & Olsen, B. D. Complex coacervation of supercharged proteins with polyelectrolytes. *Soft Matter* **12**, 3570–3581 (2016).
[21] Kishimura, A. Development of polyion complex vesicles (PICsomes) from block copolymers for biomedical applications. *Polym. J.* **45**, 892–897 (2013).
[22] Kishimura, A. et al. PH-dependent permeability change and reversible structural transition of PEGylated polyion complex vesicles (PICsomes) in aqueous media. *Soft Matter* **5**, 529–532 (2009).
[23] Oana, H., Morinaga, M., Kishimura, A., Kataoka, K. & Washizu, M. Direct formation of giant unilamellar vesicles from microparticles of polyion complexes and investigation of their properties using a microfluidic chamber. *Soft Matter* **9**, 5448–5458 (2013).
[24] Oana, H. et al. Spontaneous formation of giant unilamellar vesicles from microdroplets of a polyion complex by thermally induced phase separation. *Angew. Chemie - Int. Ed.* **48**, 4613–4616 (2009).
[25] Anraku, Y., Kishimura, A., Oba, M., Yamasaki, Y. & Kataoka, K. Spontaneous formation of nanosized unilamellar polyion complex vesicles with tunable size and properties. *J. Am. Chem. Soc.* (2010).
[26] Anraku, Y., Kishimura, A., Kobayashi, A., Oba, M. & Kataoka, K. Size-controlled long-circulating PICsome as a ruler to measure critical cut-off disposition size into normal and tumor tissues. *Chem. Commun.* **47**, 6054–6056 (2011).
[27] Koide, A. et al. Semipermeable polymer vesicle (PICsome) self-assembled in aqueous medium from a pair of oppositely charged block copolymers: Physiologically stable micro-/nanocontainers of water-soluble macromolecules. *J. Am. Chem. Soc.* **128**, 5988–5989 (2006).
[28] Anraku, Y., Kishimura, A., Yamasaki, Y. & Kataoka, K. Living unimodal growth of polyion complex vesicles via two-dimensional supramolecular polymerization. *J. Am. Chem. Soc.* **135**, 1423–1429 (2013).

[29] Hori, M., Cabral, H., Toh, K., Kishimura, A. & Kataoka, K. Robust Polyion Complex Vesicles (PICsomes) under Physiological Conditions Reinforced by Multiple Hydrogen Bond Formation Derived by Guanidinium Groups. *Biomacromolecules* **19**, 4113–4121 (2018).
[30] Mutaf, O. F., Anraku, Y., Kishimura, A. & Kataoka, K. Unilamellar polyion complex vesicles (PICsomes) with tunable permeabilities for macromolecular solutes with different shapes and sizes. *Polymer.* **133**, 1–7 (2017).
[31] Chuanoi, S., Anraku, Y., Hori, M., Kishimura, A. & Kataoka, K. Fabrication of polyion complex vesicles with enhanced salt and temperature resistance and their potential applications as enzymatic nanoreactors. *Biomacromolecules* **15**, 2389–2397 (2014).
[32] Naoyama, K., Mori, T., Katayama, Y. & Kishimura, A. Fabrication of Dendrimer-Based Polyion Complex Submicrometer-Scaled Structures with Enhanced Stability under Physiological Conditions. *Macromol. Rapid Commun.* **37**, 1087–1093 (2016).
[33] Liu, Y. et al. Inducible dynamic behavior of polyion complex vesicles by disrupting charge balance. *Chem. Lett.* **50**, 1034–1037 (2021).
[34] Kishimura, A., Koide, A., Osada, K., Yamasaki, Y. & Kataoka, K. Encapsulation of myoglobin in PEGylated polyion complex vesicles made from a pair of oppositely charged block ionomers: A physiologically available oxygen carrier. *Angew. Chemie - Int. Ed.* **46**, 6085–6088 (2007).
[35] Anraku, Y. et al. Systemically Injectable Enzyme-Loaded Polyion Complex Vesicles as in Vivo Nanoreactors Functioning in Tumors. *Angew. Chemie - Int. Ed.* **55**, 560–565 (2016).
[36] Tang, H., Sakamura, Y., Mori, T., Katayama, Y. & Kishimura, A. Development of Enzyme Loaded Polyion Complex Vesicle (PICsome): Thermal Stability of Enzyme in PICsome Compartment and Effect of Coencapsulation of Dextran on Enzyme Activity. *Macromol. Biosci.* **17**, 1–7 (2017).
[37] Zong, W. et al. A Fissionable Artificial Eukaryote-like Cell Model. *J. Am. Chem. Soc.* **139**, 9955–9960 (2017).
[38] Zong, W., Li, Q., Zhang, X. & Han, X. Deformation of giant unilamellar vesicles under osmotic stress. *Colloids Surfaces B Biointerfaces* **172**, 459–463 (2018).
[39] Vanhille-Campos, C. & Šarić, A. Modelling the dynamics of vesicle reshaping and scission under osmotic shocks. *Soft Matter* **17**, 3798–3806 (2021).
[40] Perera, R. M. et al. Influence of NaCl on shape deformation of polymersomes. *Soft Matter* **17**, 4452–4463 (2021).

[41] Salva, R. et al. Polymersome shape transformation at the nanoscale. *ACS Nano* **7**, 9298–9311 (2013).
[42] Zong, W., Zhang, X., Li, C. & Han, X. Thylakoid Containing Artificial Cells for the Inhibition Investigation of Light-Driven Electron Transfer during Photosynthesis. *ACS Synth. Biol.* **7**, 945–951 (2018).
[43] Seifert, U. Advances in Physics Configurations of fluid membranes and vesicles. *Advances in Physics vol.* **46** (1997).
[44] Mountain, G. A. & Keating, C. D. Formation of Multiphase Complex Coacervates and Partitioning of Biomolecules within them. *Biomacromolecules* **21**, 630–640 (2020).
[45] Lu, T. & Spruijt, E. Multiphase Complex Coacervate Droplets. *J. Am. Chem. Soc.* **142**, 2905–2914 (2020).
[46] Fisher, R. S. & Elbaum-Garfinkle, S. Tunable multiphase dynamics of arginine and lysine liquid condensates. *Nat. Commun.* **11**, (2020).
[47] Wibowo, A. et al. Morphology control in water of polyion complex nanoarchitectures of double-hydrophilic charged block copolymers through composition tuning and thermal treatment. *Macromolecules* **47**, 3086–3092 (2014).

Appendix 1. Polymer synthesis

Materials:

β-Benzyl-L-aspartate N-carboxy anhydride (BLA-NCA) was purchased from Chuo Kaseihin Co. Inc. (Tokyo, Japan). ε-Methoxy-α-amino-poly(ethylene glycol) (MeO-PEG-NH_2, molecular weight = 2 kDa) was purchased from Nippon Oil and Fats Co. Ltd. (Tokyo, Japan). *N*,*N*-dimethyl formamide (DMF) and Dichloromethan (DCM) were purchased from Kanto Chemical Co. Inc. (Tokyo, Japan). n-Butyl-amine (NH_2-Pr-CH_3), acetonitrile, chloroform and benzene were purchased from FUJIFILM Wako Pure Chemical Industries (Osaka, Japan). 3-amino-1-propanol (NH_2-Pr-OH) was purchased from Tokyo Chemical Industry Co., Ltd. (Tokyo, Japan). Deuterium oxide (D_2O) was purchased from MERCK KGaA (Darmstadt, Germany).

Procedure:

PEG-PAsp

First, PEG- poly(β-Benzyl-L-aspartate) (PEG-PBLA) was synthesized via ring opening polymerization using BLA-NCA as a monomer and MeO-PEG-NH_2 as an initiator (Figure S1). MeO-PEG-NH_2 was dissolved in benzene and freeze dried for overnight. Freeze dried initiator was dissolved in DMF with N_2 purging. BLA-NCA was measured in N_2 glove box and dissolved in DCM and DMF under N_2 purging such that the volume ratio of DCM and DMF is 2:1 in the final reaction mixture. Then, the monomer solution was added to the initiator solution under N_2 purging. The reaction was conducted at 40 ℃ for 48 h. The white turbid solution was then dissolved in a limited amount of chloroform and precipitated in Hexane : Ethyl acetate (6:4 v/v) solution. The polymer was collected by vacuum filtration in PTFE membrane. Retrieved polymer was re-dissolved in chloroform : benzene (1:3 v/v) and freeze dried for 2 days.

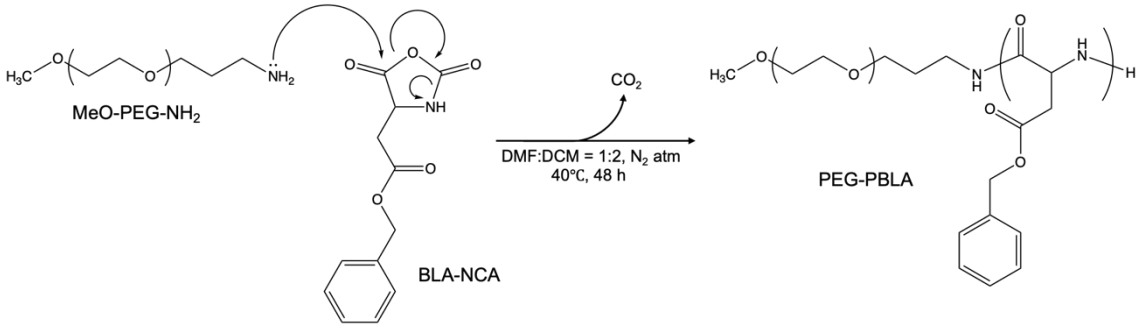

Figure S1. Synthetic scheme of PEG-PBLA via ring open polymerization.

Then, PEG-PBLA was hydrolyzed under basic condition to obtain PEG-PAsp (Figure S2). PEG-PBLA was dissolved in acetonitrile and 0.5 M NaOH was added at 5 equivalent to side chain. The mixture was stirred for 1 h at RT, followed by dialysis against distilled water for 2 days and freeze drying for another 2 days.

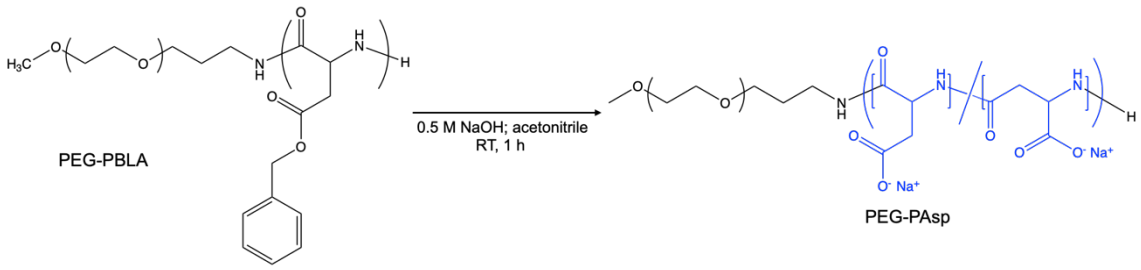

Figure S2. Hydrolysis of PEG-PBLA into PEG-PAsp.

Homo-PAsp-OH (or CH_3)

Homo-PBLA was first synthesized by using n-butyl amine as an initiator in the same protocol as PEG-PBLA synthesis. Then, the side chain of homo-PBLA was partially substituted into hydroxyl group or methyl group via aminolysis reaction (Figure S3). Homo-PBLA was reacted with NH_2-Pr-OH or NH_2-Pr-CH_3 (9 equivalent to the residual benzyl ester group in Homo-PBLA) in DMF at 35 ℃ for 1 h. After the reaction, the remained benzyl ester group was hydrolyzed in 0.5 M NaCl solution (for OH) or the mixture of acetonitrile and 0.5 M NaCl (for CH_3) for 30 min, followed by dialysis against distilled water for 2 days and freeze drying for 2 days.

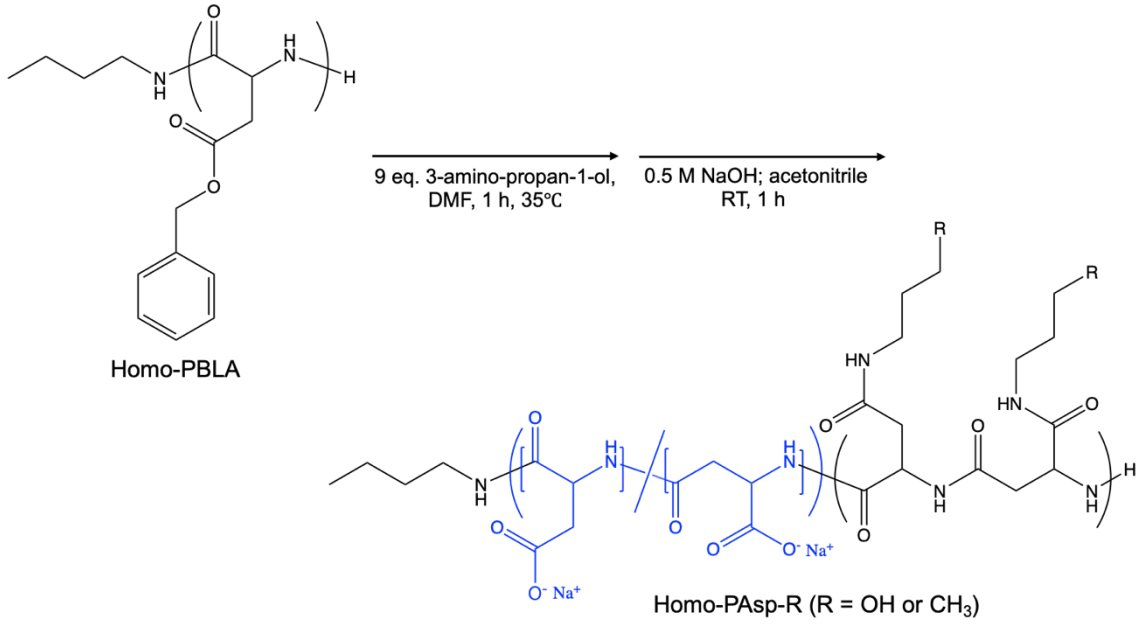

Figure S3. Partial side chain modification of Homo-PBLA via aminolysis reaction.

Result:

PEG$_{2k}$-PAsp$_{67}$

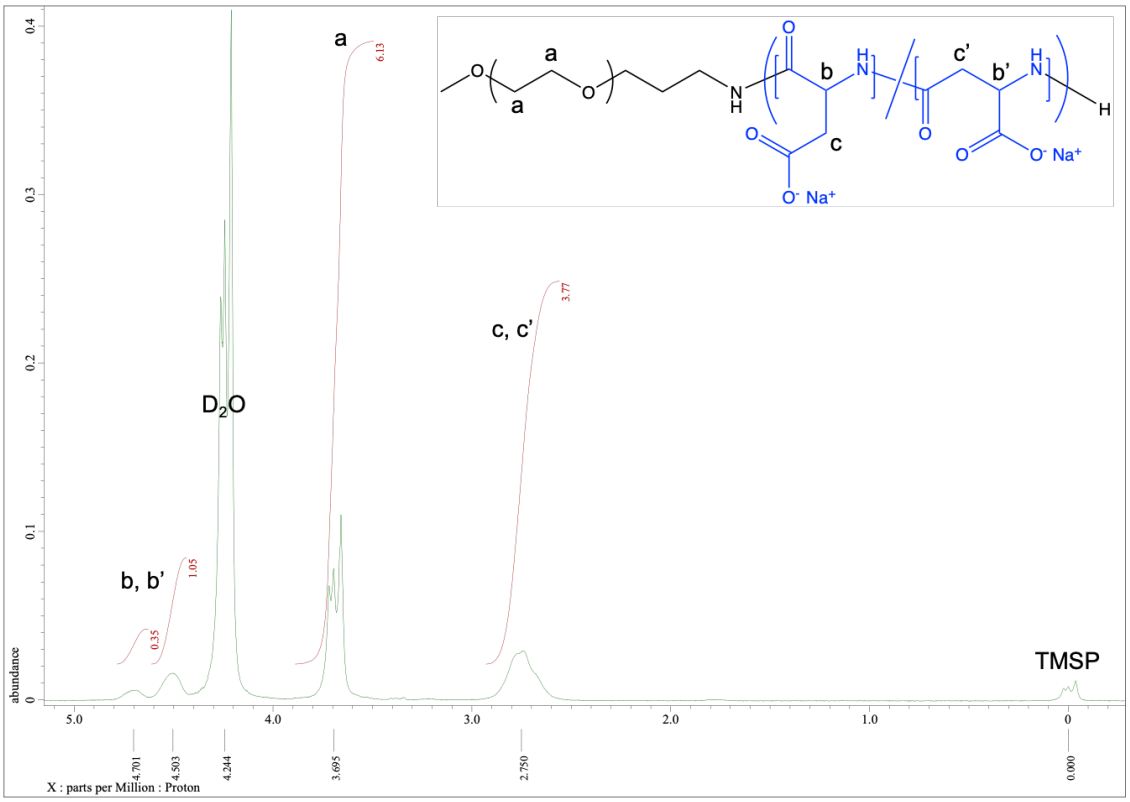

^{1}H NMR spectra of PEG$_{2k}$-PAsp$_{67}$ in D_2O at 80°C

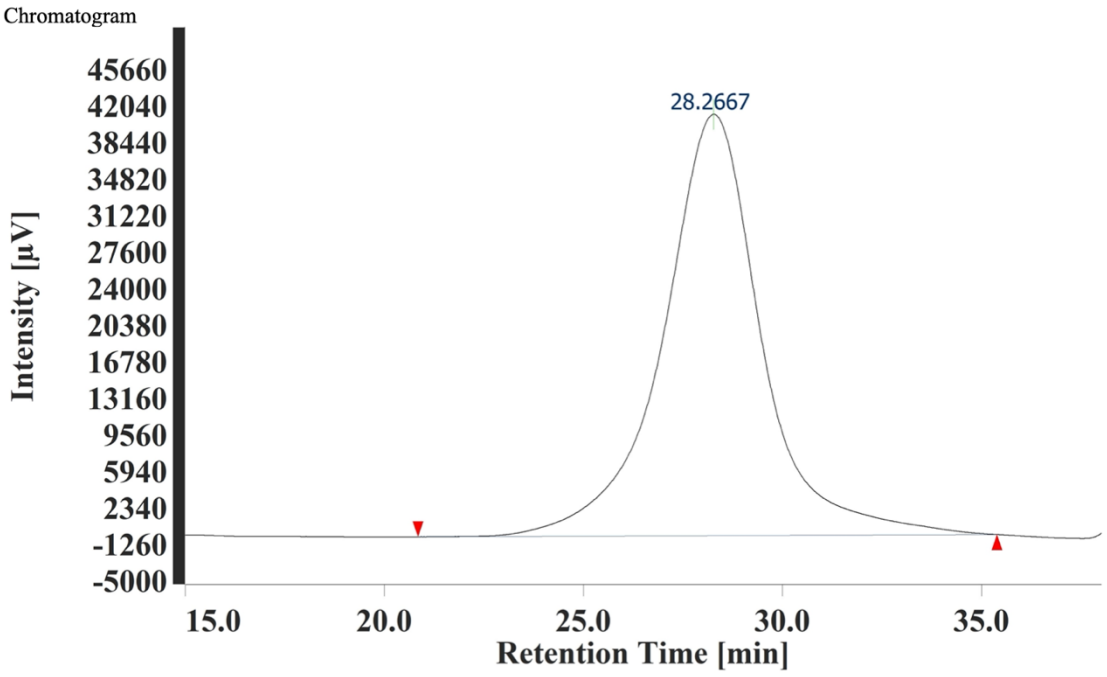

Size exclusion chromatogram of PEG$_{2k}$-PAsp$_{67}$

PEG$_{2k}$-PAsp$_{93}$

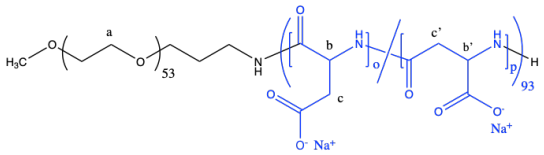

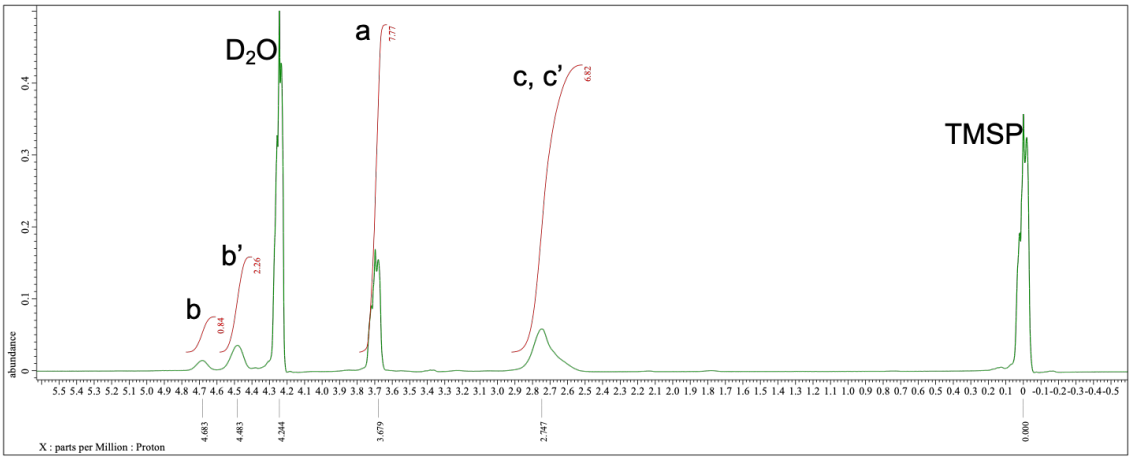

^{1}H NMR spectra of PEG$_{2k}$-PAsp$_{93}$ in D_2O at 80°C

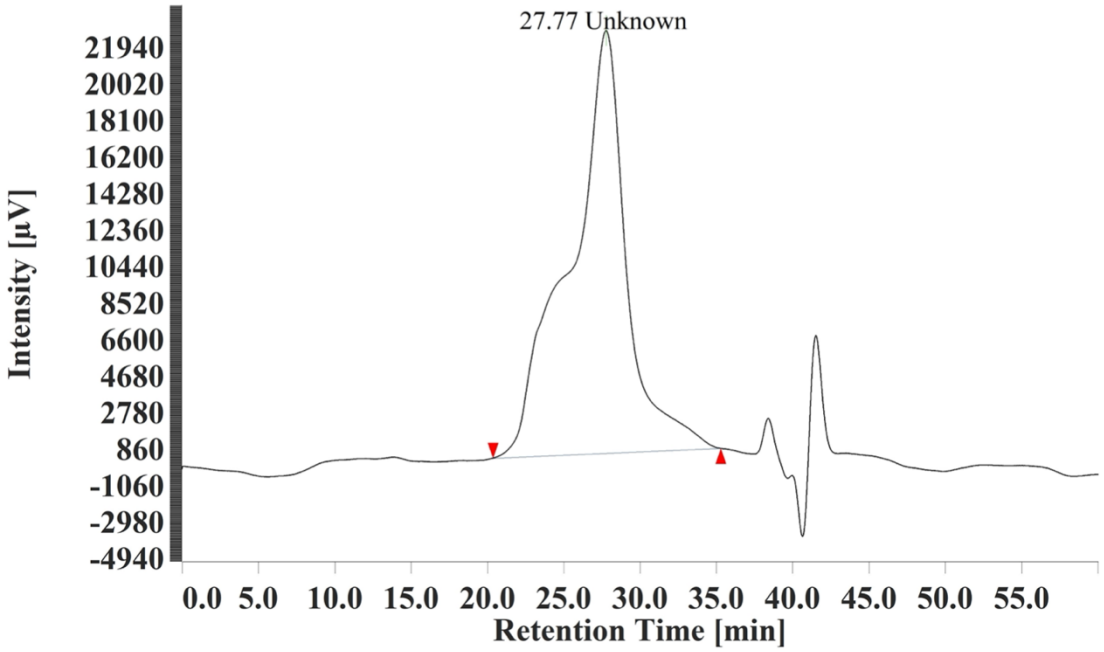

Size exclusion chromatogram of PEG$_{2k}$-PAsp$_{93}$

Homo-PAsp$_{56}$-OH$_{28}$

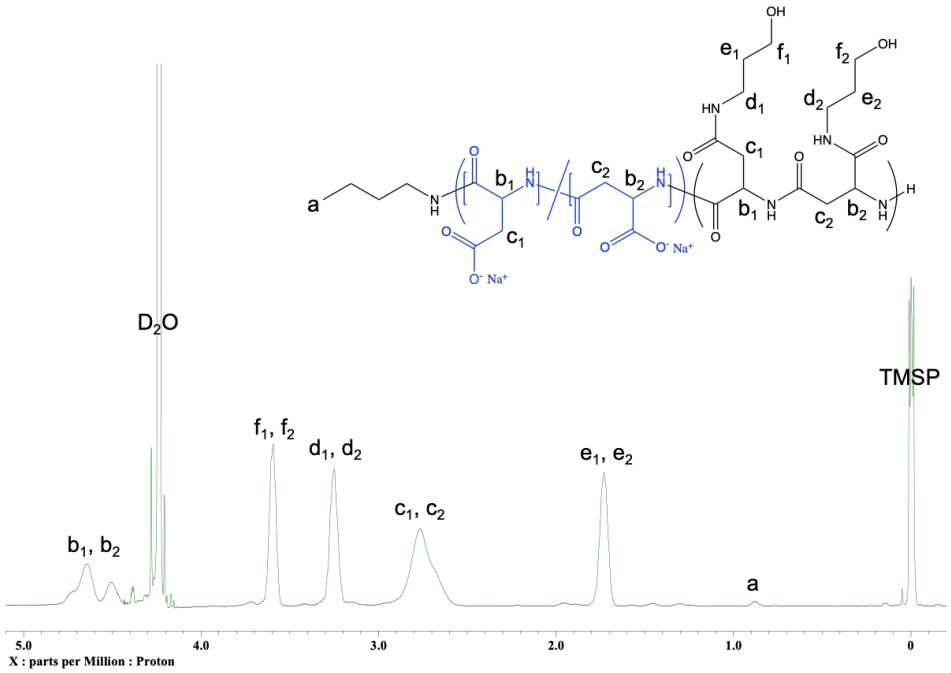

^{1}H NMR spectra of Homo-PAsp$_{56}$-OH$_{28}$ in D_2O at 80°C

Homo-PAsp$_{45}$-(CH$_3$)$_{39}$

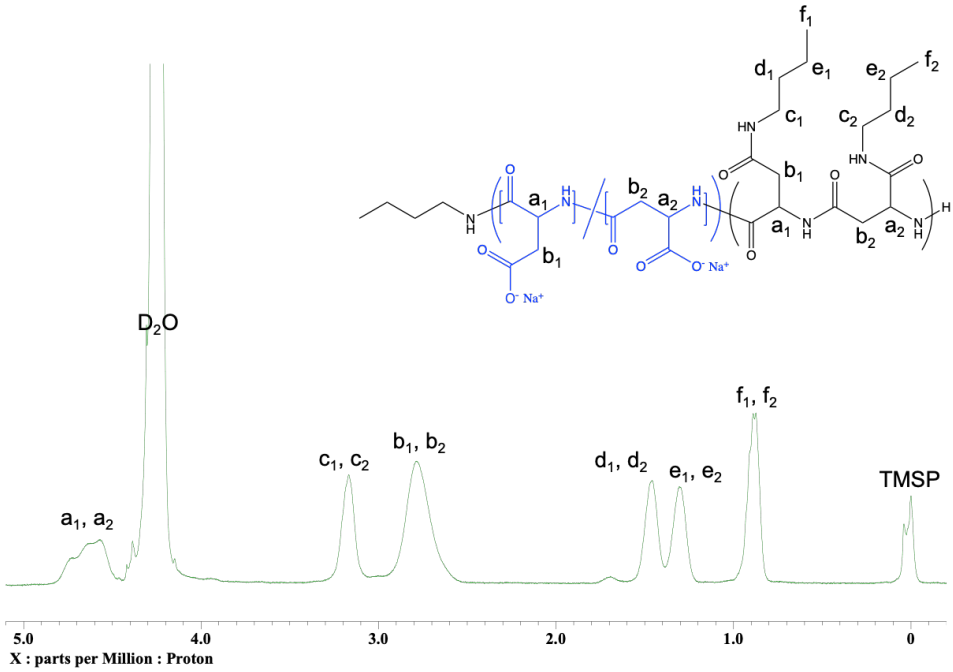

^{1}H NMR spectra of Homo-PAsp$_{45}$-(CH$_3$)$_{39}$ in D_2O at 80°C

Appendix 2. Thermodynamic stability of nested and tethered multiphase coacervate

To investigate the thermodynamic stability of nested multiphase coacervate and tethered multiphase coacervate, two polyanions were separately complexed with polycation at C/A = 1, followed by the mixing of the two mixtures. Similar to the all-at-once mixing case, this sequential mixing also formed nested multiphase coacervate and tethered multiphase coacervate (Figure S4), indicating that these coacervates are energetically stable state.

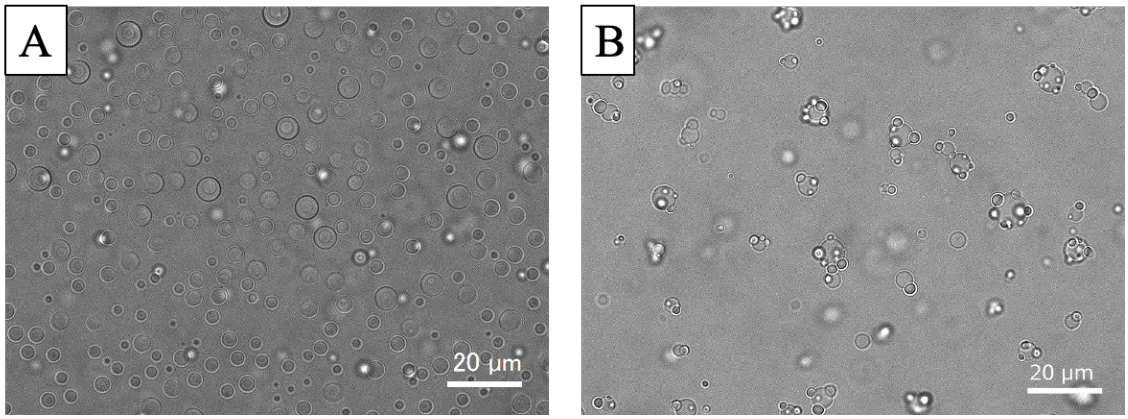

Figure S4. Optical microscopy images of (A) nested multiphase coacervate and (B) tethered multiphase coacervate formed by sequential mixing.

Appendix 3. Complexation at various f_{5k}

The effect of f_{5k} on the formation of coacervate-in-PICsome was investigated by varying f_{5k} from 0.2 to 0.5 (Figure S5). In the case of f_{5k} = 0.2, coacervate-in-PICsome was formed although a large number of PICsome co-existed, indicating that Cy3 dye was somehow involved in the favorable formation of coacervate-in-PICsome. In the case of f_{5k} = 0.3, coacervate and PICsome was totally separated and similarly in the case of f_{5k} = 0.5, coacervate, PICsome and micelle was separately co-existed. These results may be attributed that PICsome or micelle were immediately stabilized due to the existence of PEG_{5k}-PAsp prior to the formation of coacervate-in-PICsome.

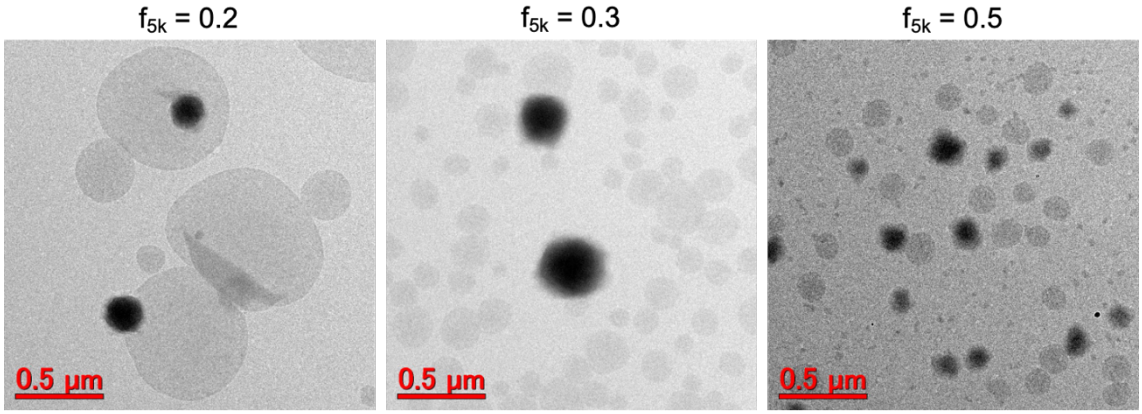

Figure S5. TEM images of PICs obtained from PEG_{2k}-PAsp, PEG_{5k}-PAsp, Homo-PAsp-CH_3 and Homo-PLL at various f_{5k}.

Appendix 4. The effect of DP on multiphase coacervation

To examine the effect of DP on multiphase coacervation, the polymer combination of Homo-PAsp$_{27}$, Homo-PAsp$_{107}$ and Homo-PLL was exploited. The formation of one phase coacervate was observed (Figure S6), which indicate that the difference of DP does not significantly affect the multiphase coacervation.

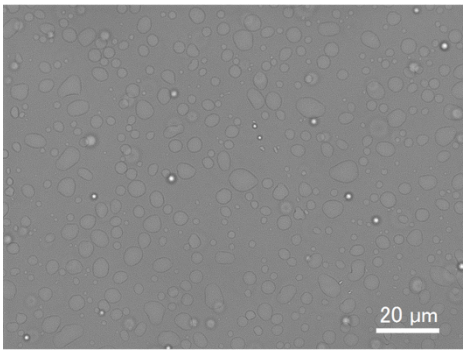

Figure S6. Optical microscopy image of PIC obtained from Homo-PAsp$_{27}$, Homo-PAsp$_{107}$ and Homo-PLL.

Appendix 5. Ternary systems with OH modified polymers

The polymer combination of Homo-PAsp, Homo-PAsp-OH and Homo-PLL was used to check the effect of reduced charge density of Homo-PAsp on the phase separation. The polymer concentration was adjusted to 5 mg/mL to prepare large coacervate for the easy observation. It was confirmed that multiphase coacervate was formed (Figure S7A), revealing that decreasing the charge density by side chain modification of one of the polyanions is effective for multiphase coacervation.

Next, the polymer combination of PEG-PAsp-OH, Homo-PAsp-OH and Homo-PLL was attempted, in which both PEG-PAsp and Homo-PAsp were modified with OH. It seemed that multiphase coacervate was formed due to the different modification ratio between PEG-PAsp-OH (37%) and Homo-PAsp-OH (67%) although the volume ratio of outer phase is very small compared to PEG-PAsp/Homo-PAsp-OH/Homo-PLL system (Figure S7B), indicating that reduction of the difference in charge density between two components leads to the formation of homogenous particles.

Finally, the polymer combination of PEG-PAsp/Homo-PAsp-OH (29%)/Homo-PLL was attempted to explore the effect of modification ratio on the complexation. The formation of one phase coacervate was confirmed (Figure S7C), showing that high modification ratio is required for the formation multiphase coacervate.

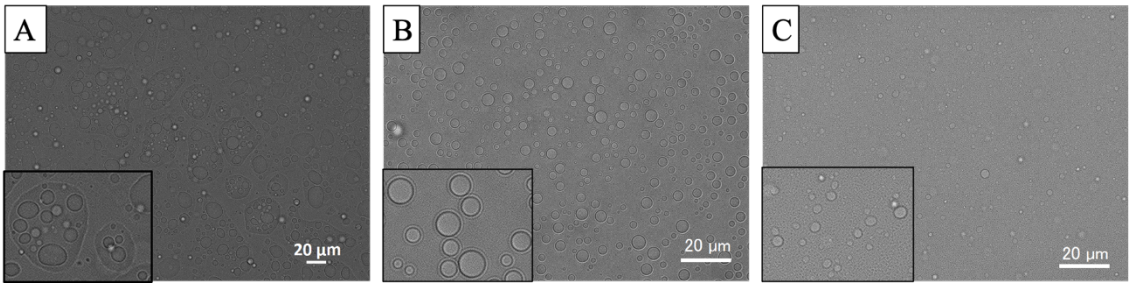

Figure S7. Optical microscopy images of PICs obtained from (A) Homo-PAsp, Homo-PAsp-OH and Homo-PLL, (B) PEG-PAsp-OH, Homo-PAsp-OH and Homo-PLL and (C) PEG-PAsp, Homo-PAsp-OH (29%) and Homo-PLL.

Appendix 6. Complexation with dendrimer

The bulky structure of dendrimer was expected to be favorable for phase separation into PICsome and coacervate. Hence, dendritic PLL with 6th generation (KG6) was used as a coacervate components and complexed with Homo-PAsp in the presence of PEG-PLL. Unfortunately, it formed the similar structure with PEG-PAsp/Homo-PAsp/Homo-PLL, meaning that the two components could not phase separate (Figure S8). It can be considered that the charge density of KG6 should be decreased in order to form coacervate-in-PICsome.

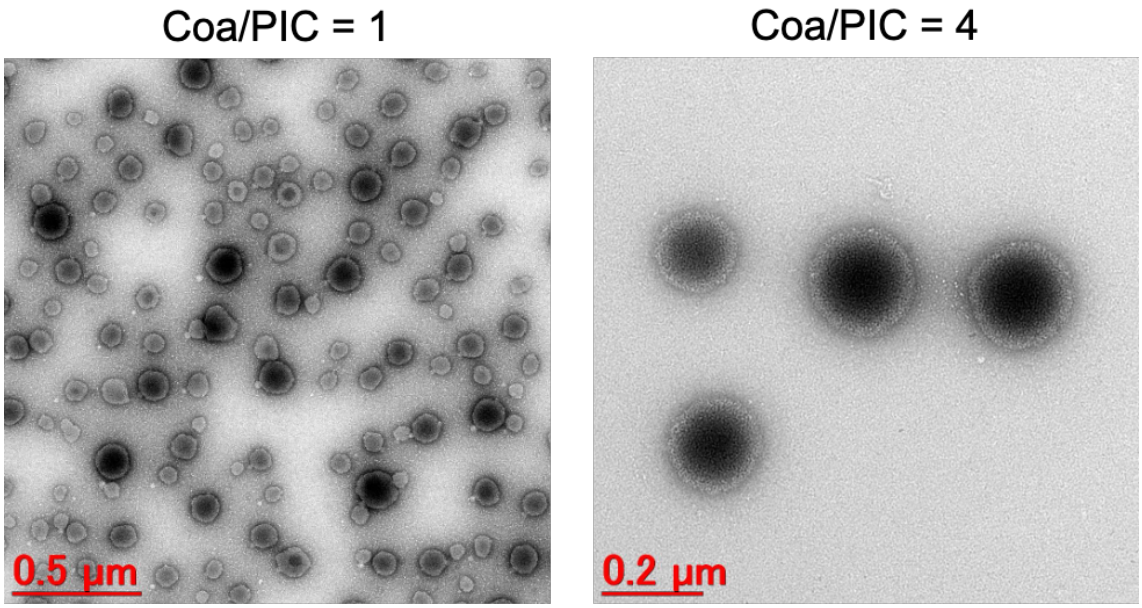

Figure S8. TEM images of PICs obtained from PEG-PLL, KG6 and Homo-PAsp.

Appendix 7. Multiphase coacervate with guanidinylated homo-PLL

Considering that multiphase coacervation occurs when two or more coacervate components have significantly different polymer interaction strength, tuning the guanidinylation ratio on homo-PLL can be a promising strategy to control the multiphase coacervation. To this end, homo-PLL with various guanidinylation ratio was exploited to form multiphase coacervate with homo-PAsp. Three types of homo-PLL, 0%, 50% and 100% guanidinylated homo-PLL were mixed in various combinations, including ternary system and quaternary system. All ternary systems formed two phase coacervate and quaternary system formed three phase coacervate (Figure S9), indicating that tuning the guanidinylation ratio can control the number of multiphase coacervate.

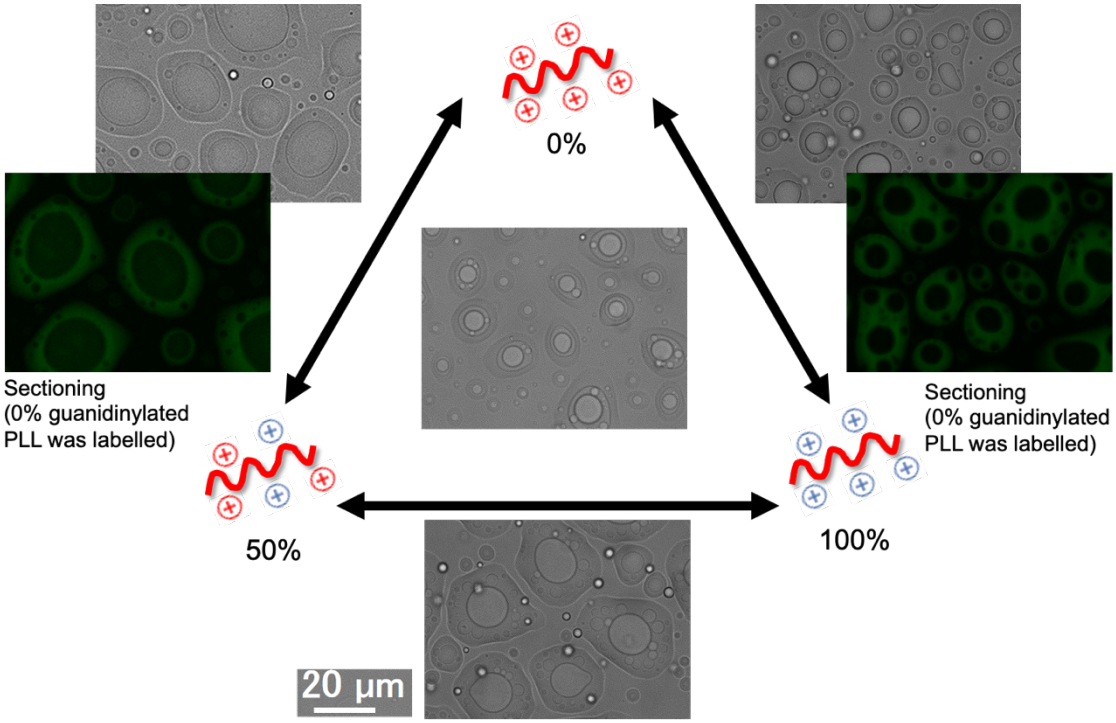

Figure S9. Optical and fluorescence microscopy images of multiphase coacervate formed from homo-PLL with various guanidinylation ratio.

Appendix 8. PEG-PG/Homo-PLL/Homo-PAsp

Increasing the polymer interaction strength of PICsome components can also be one of the ways to differentiate the polymer interaction strength between PICsome components and coacervate components for the formation of coacervate-in-PICsome. Herein, the polymer combination of PEG-PG, Homo-PLL and Homo-PAsp was attempted. However, it did not form coacervate-in-PICsome but formed the similar structure with PEG-PAsp/Homo-PAsp/Homo-PLL case (Figure S10). This result indicate that if one of the two components have too high polymer interaction strength, it may lead to the formation of homogenous particle possibly because decreased polymer mobility suppress the phase separation.

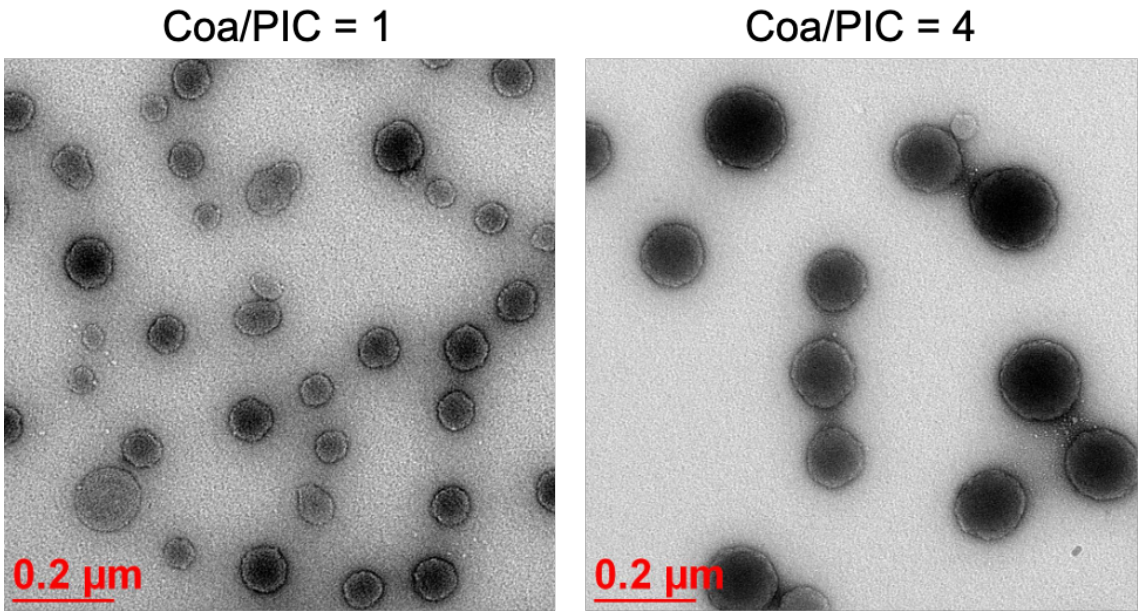

Figure S10. TEM images of PICs obtained from PEG-PG, Homo-PLL and Homo-PAsp.